



PONTIFICIA UNIVERSIDAD CATÓLICA DE CHILE  
ESCUELA DE INGENIERÍA

**ANALYSIS AND DESIGN OF TIMBER  
CONCRETE FLOORS WITH BOUNDARY  
CONDITIONS DIFFERENT THAN SIMPLY  
SUPPORTED**

**ANDRÉS IVÁN ADEMA YUSTA**

Thesis submitted to the Office of Research and Graduate Studies  
in partial fulfillment of the requirements for the degree of  
Master of Science in Engineering

Advisor:

HERNÁN SANTA MARÍA OYANEDEL

Santiago de Chile, January 2021

© 2021, ANDRÉS IVÁN ADEMA YUSTA



PONTIFICIA UNIVERSIDAD CATÓLICA DE CHILE  
ESCUELA DE INGENIERÍA

**ANALYSIS AND DESIGN OF TIMBER  
CONCRETE FLOORS WITH BOUNDARY  
CONDITIONS DIFFERENT THAN SIMPLY  
SUPPORTED**

**ANDRÉS IVÁN ADEMA YUSTA**

Members of the Committee:

HERNÁN SANTA MARÍA OYANEDEL

PABLO GUINDOS BRETONES

ALEXANDER OPAZO VEGA

DANIEL GARRIDO CORTÉS

Thesis submitted to the Office of Research and Graduate Studies  
in partial fulfillment of the requirements for the degree of  
Master of Science in Engineering

Santiago de Chile, January 2021

© 2021, ANDRÉS IVÁN ADEMA YUSTA

*Gratefully to my parents and sisters*

## AGRADECIMIENTOS

Gracias a mis padres, Christian y Sara, por ser el soporte detrás de todos mis logros personales, académicos y deportivos. Por acompañarme desde la distancia durante mi carrera universitaria, la escritura de mi tesis y cada vez que lo necesité. A mis hermanas, Ingrid y Priscila, por su apoyo, consejos y compañía incondicional.

Agradecer a los profesores Hernán y Pablo, quienes me brindaron toda su confianza, apoyo, conocimiento y disposición durante mi estadía en postgrado. Al Centro de Innovación en Madera (CIM) por hacerme parte del proyecto en el que desarrollé mi tesis, y al Departamento de Ingeniería Estructural y Geotécnica por acogerme durante mi estadía en la universidad.

Quisiera agradecer a mis amigos y compañeros de especialidad, Benjamín, Gustavo, Ilonka, Sofía y Renzo, por su apoyo y amistad que aún perdura. Darle las gracias también a Chloe por su paciencia, compañía y por haber sido un pilar fundamental durante el proceso de escritura de tesis y la cuarentena.

Finalmente, agradecer a todos quienes formaron parte de mi vida durante la universidad, familia, profesores, compañeros, amigos del colegio, selección de *handball* y entrenadores. Sin ustedes no hubiera llegado a esta instancia.

## TABLE OF CONTENTS

AGRADECIMIENTOS	iv
LIST OF FIGURES	vii
LIST OF TABLES	ix
ABSTRACT	x
RESUMEN	xi
1. INTRODUCTION	1
1.1. Background and Problematic . . . . .	1
1.2. Hypothesis . . . . .	2
1.3. Objectives . . . . .	3
1.4. State of the art . . . . .	3
1.4.1. Shear connectors . . . . .	5
1.4.2. Short term behavior . . . . .	6
1.4.3. Long term behavior . . . . .	8
2. MODEL EXPLANATION	11
2.1. $\gamma$ - method . . . . .	11
2.2. Girhammar method . . . . .	13
2.3. Long-term simplified model . . . . .	16
2.4. Finite Element Modeling . . . . .	19
2.4.1. Elements used . . . . .	20
2.4.2. Connection system . . . . .	21
2.4.3. Concrete shrinkage . . . . .	22
2.4.4. Creep . . . . .	22
3. NUMERICAL AND EXPERIMENTAL VALIDATION	25
3.1. Section Design and Material Properties . . . . .	25

3.2. Short term behavior . . . . .	26
3.3. Long term behavior . . . . .	30
3.4. Experimental validation . . . . .	34
4. PROPOSAL OF DESIGN PROCEDURE	43
4.1. Design example . . . . .	47
4.1.1. Basic information . . . . .	48
4.1.2. Verification of the ultimate limit state at the short-term . . . . .	51
4.1.3. Verification of the ultimate limit state at the long-term . . . . .	54
4.1.4. Verification of the serviceability limit state at the short-term . . . . .	56
4.1.5. Verification of the serviceability limit state at the long-term . . . . .	57
5. CONCLUSIONS	59
REFERENCES	61
APPENDIX	68
A. ELASTIC ANALYSIS OF INELASTIC STRAINS . . . . .	69
B. COMPARISON OF CREEP MODELS FOR CONCRETE AND TIMBER . . . . .	74

## LIST OF FIGURES

1.1	Influence of the stiffness of the connection in a TCC. . . . .	4
1.2	Comparisons of different categories of connection systems . . . . .	6
1.3	Examples of timber-concrete connections. . . . .	7
1.4	Finite element model proposed by Fragiacommo . . . . .	10
2.1	Cross section (left) and stress distribution (right) of a TCC. . . . .	12
2.2	Approximate deflection expressions for beams with different loads and boundary conditions . . . . .	15
2.3	Creep coefficients of timber considering different values of $\Delta u$ . . . . .	20
2.4	Deflections in five years induced by concrete shrinkage for different support conditions. . . . .	23
3.1	Slab design. . . . .	26
3.2	Simply supported beam long term maximum deflection at mid-span. . . . .	31
3.3	Propped cantilever beam long term maximum deflection. . . . .	32
3.4	Long term deflection (5 years). . . . .	33
3.5	Long term deflection (50 years). . . . .	34
3.6	Slab design. . . . .	35
3.7	Ansys NL and Ansys L model. . . . .	37
3.8	Deflection of the PT beam. . . . .	39
3.9	Comparison of maximum deflection calculated with the Proposed analytical model and Ansys L model. . . . .	41

3.10	Slip along the beam at 80 kN Load. . . . .	42
4.1	Cross section (left) and stress distribution (right) of a TCC. . . . .	45
4.2	Summary of the proposed design procedure for the Ultimate Limit States. . .	46
4.3	Summary of the proposed design procedure for the Serviceability Limit States.	47
4.4	Slab design. . . . .	48
4.5	Moment and shear diagram of a propped cantilever beam. . . . .	51
A.1	Differential element of a TCC subjected to axial deformations of each component. . . . .	69
B.1	Concrete creep model comparison for five years. . . . .	74
B.2	Timber creep and mechanosorptive creep model comparison for five years. . .	75
B.3	Concrete creep model comparison for fifty years. . . . .	76
B.4	Timber creep and mechanosorptive model comparison for fifty years. . . . .	77

## LIST OF TABLES

3.1	Maximum deflection comparison under different support conditions for service loads. . . . .	26
3.2	Instantaneous deflection for a propped cantilever beam subjected to service loads. . . . .	27
3.3	Stresses for a propped cantilever beam subjected to service loads. . . . .	28
3.4	Interlayer force along the x axis for the different models. . . . .	30
3.5	Timber and concrete properties. . . . .	36
3.6	PT connection properties from tests. . . . .	36
3.7	Summary of the models. . . . .	38
4.1	Comparison between the proposed design procedure and the EC5 design procedure. . . . .	43
B.1	Constant values for concrete creep model for five years. . . . .	74
B.2	Constant values for timber creep and mechanosorptive creep model for five years. . . . .	75
B.3	Constant values for concrete creep model for fifty years. . . . .	76
B.4	Constant values for timber creep and mechanosorptive creep model for fifty years. . . . .	77

## ABSTRACT

This thesis describes an analytical procedure for designing timber concrete composites (TCC) subjected to boundary conditions different than simply supported. Currently available investigations of TCCs are mainly focused on simply supported slabs, as it is a typical configuration for timber buildings. However, in other structural applications, and remarkably for reinforced concrete buildings, the boundary conditions of the TCC slabs are not likely to be simply supported. Such distinct boundary conditions can significantly reduce the cross section height, mid-span deflection and self weight of the structure, the last one being crucial in seismic regions. The proposed procedure is derived from two simplified methods available in the literature, one being general in its nature while the other being valid for simply supported beams. The short-term analytical model was compared against finite element models (FEM) and to the only experimental investigation available in the literature, while the long-term analytical model was compared only against FEM. In the last section, the proposed procedure is explained through a design example. It was concluded that the prediction of the models was satisfactory. Further experimental campaigns are needed in the future to assess the versatility of the model in a wider range of boundary conditions, including short-term and long-term tests, which should enhance the applicability of TCC slabs in structures different from timber buildings and bridges.

**Keywords:** Timber-concrete composite, beam, slab, Load-deflection, short-term, design.

## RESUMEN

En esta tesis se propone un procedimiento analítico para diseñar losas madera-hormigón sujetas a condiciones de borde distintas a simplemente apoyadas. Las investigaciones existentes sobre losas madera-hormigón se enfocan principalmente en condiciones de simple apoyo, lo cual es muy común en edificios de madera. Sin embargo, en otras aplicaciones estructurales, y específicamente para edificios de hormigón armado, es poco probable que las losas estén simplemente apoyadas. Este cambio en las condiciones de apoyo puede reducir de manera significativa el espesor total de la sección, deflexión máxima y peso propio de la estructura, lo cual resulta crucial en países sísmicos. El procedimiento propuesto se derivó de dos modelos simplificados existentes en la literatura, uno que se puede aplicar para cualquier condición de borde y el otro solo para la condición simplemente apoyada. El modelo analítico para el comportamiento a corto plazo se comparó con modelos de elementos finitos (FEM) y con la única investigación experimental existente en la bibliografía, mientras que el modelo analítico para el comportamiento a largo plazo se comparó solo con FEM. En el último capítulo, se muestra el procedimiento propuesto a través de un ejemplo de diseño para un edificio habitacional considerando la normativa chilena e internacional. La predicción de los modelos analíticos entregó resultados muy cercanos a los de los modelos FEM. Se concluyó que se necesitan más campañas experimentales para validar el procedimiento de diseño para un amplio rango de condiciones de borde, incluyendo comportamiento a corto y largo plazo, lo cual debiera mejorar la aplicabilidad de las losas madera-hormigón para estructuras diferentes de edificios de madera y puentes.

**Palabras Claves:** Losas madera-hormigón, carga-deflexión, corto plazo, largo plazo, diseño.

# **1. INTRODUCTION**

## **1.1. Background and Problematic**

Timber concrete composites (TCC) floors consist in a concrete slab connected to the timber below by shear connectors. Initially, the main TCC application was the upgrading of existing timber floors by adding nails and a concrete layer, specifically after World Wars I and II due to the shortage of reinforcement steel bars (Yeoh, Fragiaco, & Deam, 2011). Nowadays, TCC can be used in renovation of old timber structures, construction of new bridges (Rodrigues, Dias, & Providência, 2013) and in multi-story buildings (Ceccotti, 2002).

One of the principal advantages of using a TCC is that the concrete component depth can be reduced by about 50 % compared to a customary concrete slab (R. Gutkowski, Brown, Shigidi, & Natterer, 2008), reducing the carbon footprint and decreasing the self weight of the structure. The above becomes crucial in seismic regions since lighter floors can reduce the lateral strength required in a structural system (Yeoh, Fragiaco, De Franceschi, & Heng Boon, 2011). Additionally, it does minimize the use of formwork and props, considering that timber can perform as a structural element and as a formwork, which allows for a higher degrees of prefabrication. All this together, makes TCCs as an attractive solution for conventional reinforced concrete buildings, especially those of seismic regions.

The use of TCC floors under simply supported conditions has been widely studied by several authors through experimental investigations (Jiang & Crocetti, 2019; Ceccotti, Fragiaco, & Giordano, 2007; Mudie, Sebastian, Norman, & Bond, 2019; Yeoh, Fragiaco, & Deam, 2011; Fragiaco, 2012) or numerical/analytical ones (Fragiacomo & Ceccotti, 2006a; Khorsandnia, Valipour, & Crews, 2014; A. M. Dias, Van de Kuilen, Lopes, & Cruz, 2007; Zona, Barbato, & Fragiaco, 2012). The main objective of that

research, was to measure the short-term behavior, the long-term behavior, the mechanical properties of the connection as well as predicting the stresses, deflections and internal forces with numerical or analytical methods.

It has been stated that the main limitation of the TCC, and often the indicator which controls the design, is the mid-span deflection (Khorsandnia, Valipour, Shrestha, Gerber, & Crews, 2013; Yeoh, Fragiacom, De Franceschi, & Heng Boon, 2011). To minimize the mid-span deflection it has been recommended the use of low-shrinkage concrete and pre-cambering the timber before casting the concrete (Fragiacomo, Gutkowski, Balogh, & Fast, 2007; Tannert, Endacott, Brunner, & Vallée, 2017; Yeoh, Fragiacom, De Franceschi, & Heng Boon, 2011). However, even applying such improvements, the TCCs typically results in thicker and economically more expensive slabs in comparison to a conventional reinforced concrete slab.

Even though the assumption of simply supported condition does not usually represent the real support conditions that the TCC will be subjected to, research about the behavior of TCC under different boundary conditions is scarce (A. Dias, Schänzlin, & Dietsch, 2018). Since the TCC slabs supported on reinforced concrete wall buildings are connected to the shear walls using steel reinforcement, the behavior obtained through the analysis assuming simply supported conditions would not be accurate.

For the reasons mentioned above, a new design method for TCC was investigated. It has to be said that no previous research has aimed the design of TCC floors under boundary conditions different than simply supported.

## **1.2. Hypothesis**

The short and long term behavior of a timber-concrete slab under support conditions different than the traditional ones, such as a clamped end, can be correctly predicted with analytical methods available in the literature.

### **1.3. Objectives**

The main objective of this research is to develop an analytical procedure for analysis and design of TCC floor slabs under boundary conditions different than simply supported, considering the short term and long term behavior, the influence of the environmental conditions, different load states and the behavior of the timber to concrete connectors.

The specific objectives are:

- (i) To implement an analytical design method for the short term and long term behavior, based on existing models in the literature.
- (ii) To validate the method through comparison with numerical models.
- (iii) To validate the method through comparison with test results available in the literature.
- (iv) To design a TCC slab for a residential building in Chile using the proposed procedure.

### **1.4. State of the art**

After World Wars I and II, due to the shortage of reinforcement steel bars, the existing timber floors began to be upgraded by adding nails and a concrete layer (Yeoh, Fragiacom, & Deam, 2011). Since then, the use of TCC structures have been used not only for upgrading existing floors, but also for the construction of new buildings or bridges. As an example, in 1999 was constructed the Vihantasalmi Bridge in Finland, a 14 m wide and 168 m long road bridge, which is part of the more than 100 TCC bridges that exist worldwide (Balogh, Fragiacom, Gutkowski, Atadero, & Ivanyi, 2013).

The advantage of the TCCs is that both concrete and timber are being used more efficiently, since the concrete is subjected to compression and the timber is subjected to tension and bending. This allows to reduce the depth of the concrete component by up to 50 % compared to a solid concrete slab (R. Gutkowski et al., 2008). Since the cracked

lower part of a pure concrete slab is significantly reduced by adding the timber component, the corrosion of the steel reinforcement due to moisture penetration is not an issue in the TCCs (Lukaszewska, 2009).

In order to understand the behavior of a TCC, the interaction of the three main components have to be considered. As mentioned before, when a TCC is subjected to a load, the timber member experience bending and tensile stresses, and the concrete member experiences mainly compression. The main purpose of the connection is to transfer the longitudinal shear force between the concrete and the timber.

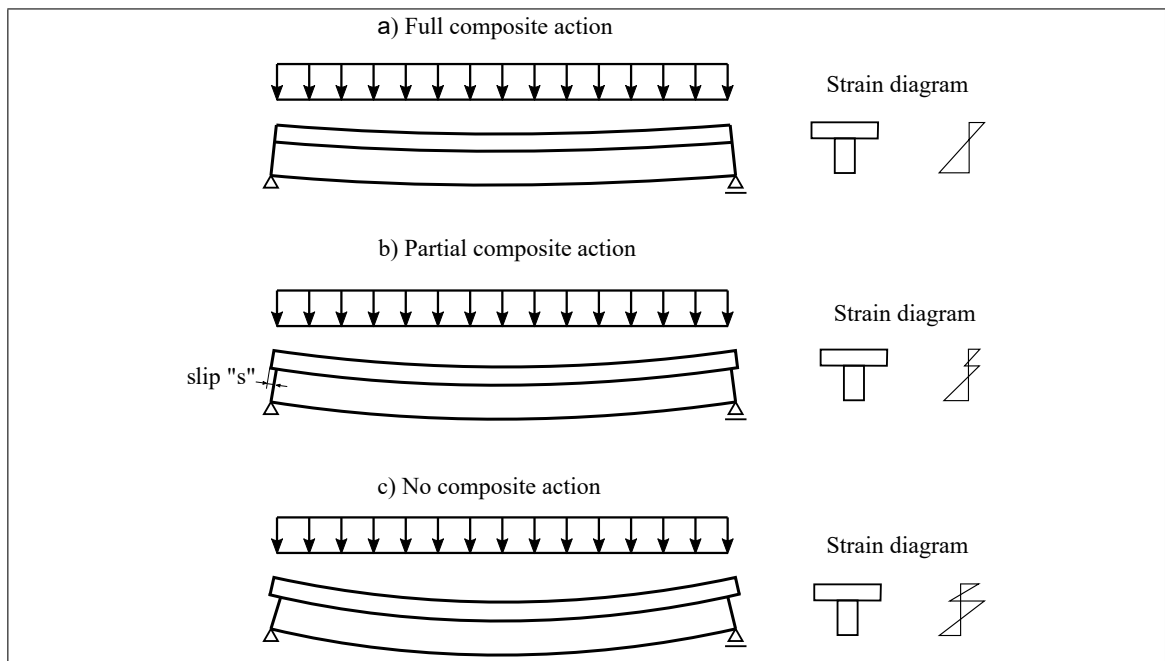


Figure 1.1. Influence of the stiffness of the connection in a TCC.

As it can be seen in Figure 1.1, there are two limits of the composite action: the upper limit, which is when the connection ensures full composite action and the concrete is rigidly connected to the timber; and the lower limit, which is when there is no composite action, and the timber and concrete work independently. In practice, a full composite action is almost impossible to reach due the flexibility of the connection (Clouston &

Schreyer, 2008), which gives way to a relative horizontal displacement, or "slip". This behavior is called "partial composite action".

The efficiency of the design highly depends of the connection stiffness. A connection system which achieves a high degree of composite action, allows to obtain longer span lengths and significantly smaller depths compared to a non composite action (Yeoh, Fragiaco, De Franceschi, & Heng Boon, 2011). The efficiency is usually measured by the quantity  $E$ ,

$$E = \frac{\Delta_{NC} - \Delta_{PC}}{\Delta_{NC} - \Delta_{FC}} \cdot 100 \quad (1.1)$$

where  $\Delta_{NC}$ ,  $\Delta_{PC}$  and  $\Delta_{FC}$  are the mid-span deflection for the cases of no composite action, partial composite action and fully rigid connection, respectively (R. M. Gutkowski, Balogh, & To, 2010).

#### **1.4.1. Shear connectors**

The connections between timber and concrete have been widely studied, since their characteristics and behavior are responsible of the main mechanical properties of the TCCs, such as composite stiffness, ductility, short-term and long-term deflections and load capacity. Due to the wide variety of connectors available, it is hard to define an ideal connection. Nevertheless, the ideal connection should be strong enough to transmit the shear force produced between the concrete and timber, stiff enough to transmit the force without involving large slips, and ductile enough to prevent the failure in the connectors and distribute the loads between the timber and concrete along the element (A. Dias et al., 2018).

Different types of connection systems have been investigated so far. They can be classified by their components as metal dowels, fasteners and screws, notches, notches with fasteners, glued connections, steel plates and others, or by their mechanical properties, as

it was done by Yeoh, Fragiacom, Franceschi and Heng Boon (2011) and shown in Figure 1.2. Moreover, they can be distinguished as discrete or continuous, vertical or inclined, adhesive or mechanically bonded, and others.

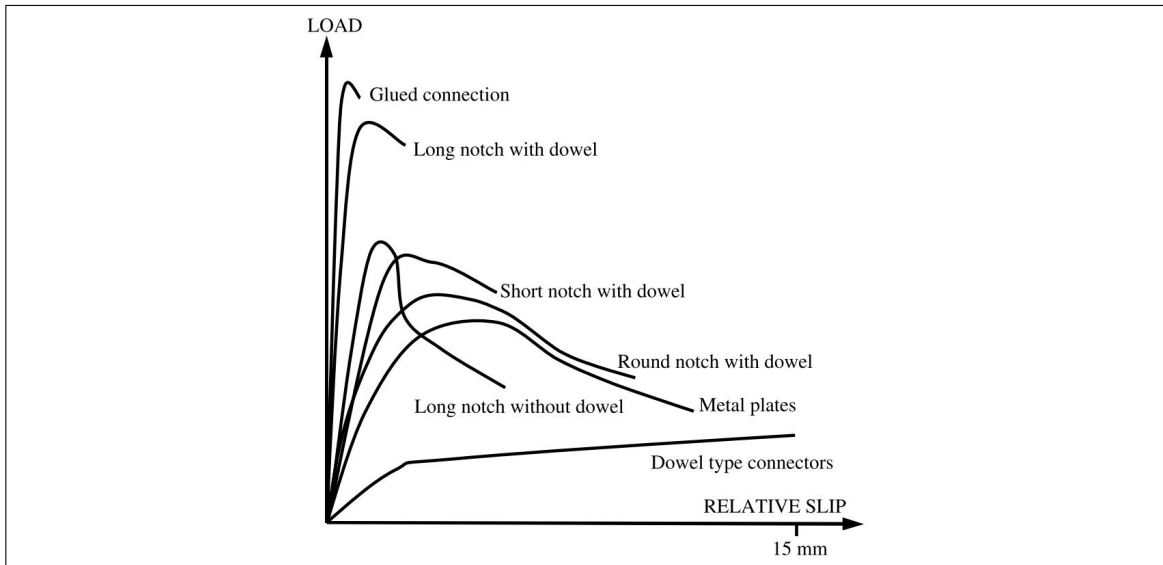


Figure 1.2. Comparisons of different categories of connection systems (Yeoh, Fragiacom, De Franceschi, & Heng Boon, 2011).

According to Dias et al.(2018), most of the studies are focused on dowel type fasteners (45 %). The studies about notches and notches combined with steel fasteners represent 33%, and other connections systems like nail plates, glued connections, friction systems, among others, represent approximately 22 % of the studies. Some of this systems are shown in Figure 1.3. The performance of the connectors is directly influenced by the concrete type and the presence of an intermediate layer (Marchi, 2018), and in the case of notched connections, by the type of timber.

#### 1.4.2. Short term behavior

Although the application of TCCs already started in central Europe by the 30s, the short term behavior of TCCs under simply supported conditions still has been quite studied the last few years. The investigations usually start with a push-out test of the connection,

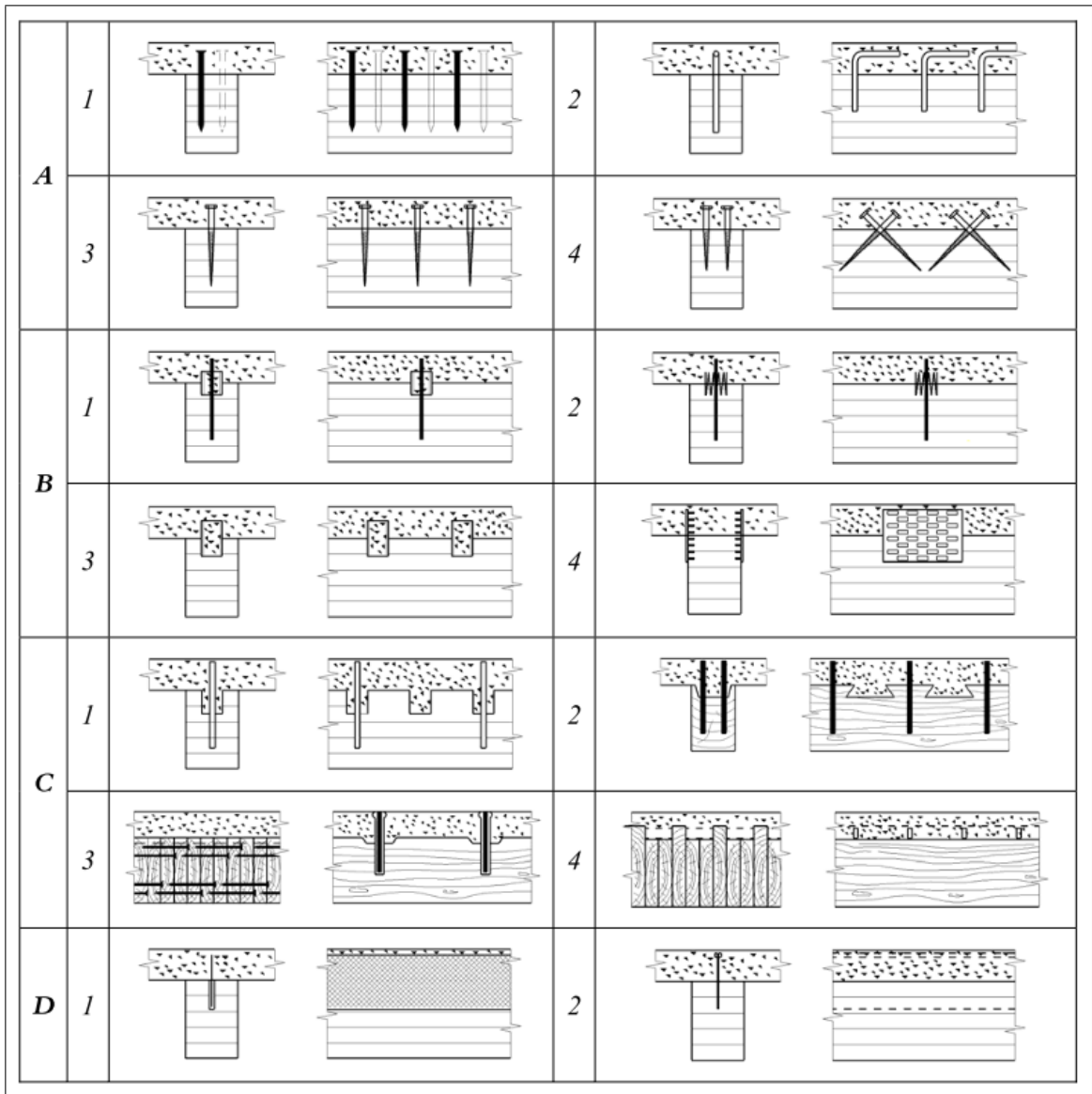


Figure 1.3. Examples of timber-concrete connections. At the letter A, it can be observed nails (1), glued reinforced steel bars (2), screws (3) and inclined screws (4). At the letter B, it can be observed split rings (1), toothed plates (2), steel tubes (3) and steel punched metal plates (4). At the letter C, round notches in timber with fasteners (1), square notches with fasteners (2), cup notches with prestressed steel bars (3) and nailed timber planks and steel shear plates (4). At the letter D it can be observed a steel mesh glued to the timber (1) and a steel plate glued to the timber (2). (Lukaszewska, 2009)

followed by a full-scale bending test loaded to failure, with the objective of quantifying the actual composite action of the system, failure mechanisms and load-bearing capacity; see for example (Brunner, Romer, & Schnüriger, 2007; R. Gutkowski et al., 2008; Lukaszewska, Fragiaco, & Johnsson, 2010; Yeoh, Fragiaco, & Deam, 2011; Khorsandnia, Valipour, Schänzlin, & Crews, 2016; Boccadoro, Zweidler, Steiger, & Frangi, 2017; Müller & Frangi, 2018). It must be noted that none of the mentioned investigations consider boundary conditions different than simply supported.

The only experimental tests considering external indeterminacy in the longitudinal direction were conducted by Sebastian et al. (2016). They tested two propped cantilever TCC beams up to failure, to understand the behavior of external indeterminacy in the longitudinal direction with presence of cracked concrete zones and changes in the connection behavior (Sebastian et al., 2016). They observed that the beams primarily failed due to connection fracture, and secondly by rupture of the LVL at the positive moment zone. None analytical nor numerical models were reported concerning the test results.

Regarding the theoretical investigations, Girhammar (2006) proposed a simplified method for designing composite beams with interlayer slip subjected to arbitrary boundary or loading conditions. This method lead to identical results than the ones obtained with the equations proposed by Eurocode 5 1-1 (European Committee for Standardization, 1995), which are based on the widely spread  $\gamma$ - method, for estimating the maximum deflection of a simply supported TCC beam. On the other hand, it was found that the use of Eurocode 5 procedure can lead to errors up to 27 % for other boundary conditions (Girhammar, 2009). It has to be mentioned that this method has not been validated with experimental campaigns regarding TCCs subjected to boundary conditions different than simply supported.

### **1.4.3. Long term behavior**

The main limitation of the TCC, and usually the indicator which controls the design, is the total long-term mid-span deflection (Khorsandnia et al., 2013; Yeoh, Fragiaco,

Buchanan, & Gerber, 2009). Since concrete and timber has different rheological behavior, it becomes necessary to include this aspect in the design. Several authors have performed long-term bending tests in order to study the behavior of TCCs.

In 2006, two 10 m long beams were tested in outdoor conditions during 430 days. It was concluded that pre-cambering the beams was imperative due the large deflections, and that the environmental changes affect the mid-span deflection (Bathon & Bletz, 2006). Fragiacomò (2007) tested eight deck systems during 133 days, in uncontrolled environmental conditions. It was concluded that the effect of concrete shrinkage is quite important, and that if a mid-span deflection limit is required, the use of low shrinkage concrete and pre-cambering is recommended.

It has been found that long-term behavior of TCC floors is not easy to predict with simple models, as it involves several phenomena such concrete shrinkage, creep and thermal strains of concrete, timber creep, changes in moisture content of timber and creep of the connection. Approximate analytical formulas, like the one proposed by Eurocode 5-Part 1-1 and 2 (European Committee for Standardization, 1995, 2011), underestimate the long term deflection of a TCC floor (Fragiacomò et al., 2007). The reason is that they usually neglect effects such as timber and connection mechanosorptive creep and concrete shrinkage (Fragiacomò, 2006; Ceccotti et al., 2007).

In order to predict the long term behavior, different authors have proposed analytical and numerical procedures to represent accurately the strains, slip and specifically the deflection. Ceccotti (2002) proposed the use of the Effective Modulus method. The method consists in reducing the modulus of elasticity of the timber and concrete to account the effects of creep. This method disregards the effects of concrete shrinkage and inelastic strains due to environmental variations, therefore it underestimates the final mid-span deflection (Yeoh, Fragiacomò, De Franceschi, & Heng Boon, 2011).

Fragiacomo and Ceccotti (2006) developed a numerical model which was validated and calibrated with experimental data. The procedure consists in a uniaxial finite element (FE) model which applies to simply supported TCCs. The model consists in a lower timber beam and an upper concrete beam joined by links which represent the connection, as is displayed in Figure 1.4. It takes into account all time-dependent phenomena mentioned earlier, and it considers data such as the daily environmental relative humidity, daily moisture content and daily and yearly thermal variations. However, such a specific approach is not suitable for design, so a simplified method was proposed, demonstrating its accuracy through comparisons with experimental data (Fragiacomo & Ceccotti, 2006a; Fragiaco, 2006). A more detailed explanation of the method will be presented in 2.3.

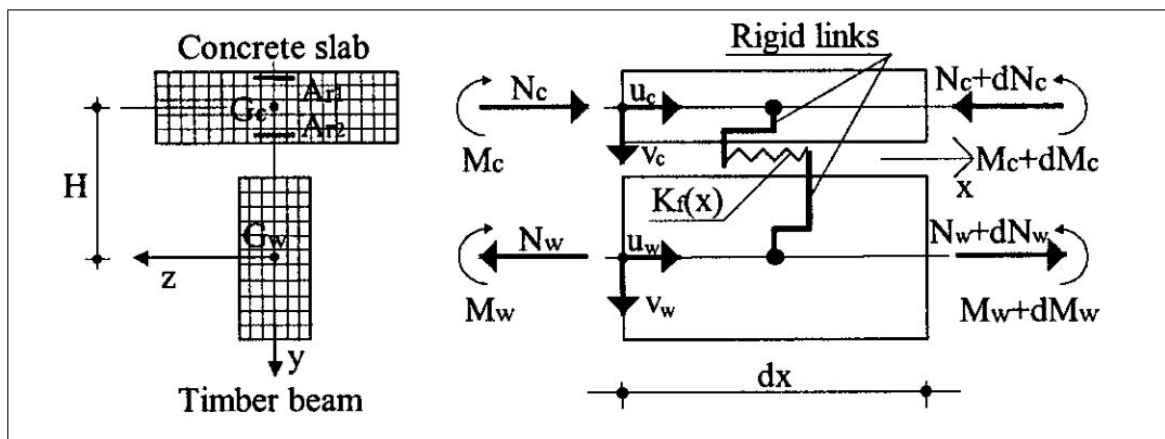


Figure 1.4. Finite element model proposed by Fragiaco and Ceccotti (Fragiacomo & Ceccotti, 2006a).

## 2. MODEL EXPLANATION

In this section the models used in this thesis for the analysis are explained. The  $\gamma$ -method and the Girhammar method are explained first, followed by an explanation of the analytical method used to predict the long-term behavior. Finally, the Finite Element Models used to validate the analytical models are described.

### 2.1. $\gamma$ - method

The  $\gamma$ - method is one of the most used methods for designing composite structures, and it has been proved by several authors that provides a reasonably good prediction of the deflection, stresses and slip under simply supported conditions (Yeoh, Fragiaco, & Deam, 2011; Tannert, Ebadi, & Gerber, 2019). The design equations can be found in the Eurocode 5-Part 1-1 Annex B (European Committee for Standardization, 1995).

The method is based on the linear elastic theory for a simply supported beam with a span  $L$ , connecting the concrete and timber by mechanical fasteners with a slip modulus  $K$  and spacing between them  $s$ .

As it has been said, the connection between the timber and concrete does not provide a perfectly bonded connection, hence the assumption of plane sections remaining plane is not valid in the full section, yet it is assumed for each component of the composite beam.

With the assumptions mentioned before, the  $\gamma$ -method defines an Effective Stiffness,  $EI_{eff}$ , which considers the stiffness provided by the shear connectors in the interface between the components of the TCC. In order to address this effect, the  $\gamma$  factor ranges between 0 (non composite action) to 1 (full composite action).

The equations of the method can be written in accordance to Figure 2.1

$$EI_{eff} = \sum_{i=1}^2 (E_i I_i + \gamma_i E_i A_i a_i^2) \quad (2.1)$$

$$\gamma_1 = 1 + \pi^2 \frac{E_1 A_1 s}{k L^2} \quad (2.2)$$

$$\gamma_2 = 1 \quad (2.3)$$

$$a_1 = \frac{h_1 + h_2}{2} - a_2 \quad (2.4)$$

$$a_2 = \gamma_1 \frac{E_1 A_1 (h_1 + h_2)}{2 (\gamma_1 E_1 A_1 + E_2 A_2)} \quad (2.5)$$

where  $s$  is the spacing between the connectors,  $L$  is the length of the beam,  $k$  the slip modulus of the connection,  $E_i$ ,  $A_i$  and  $I_i$  are the elastic modulus, area and second moment of area of the  $i$  component. The subscripts  $i = 1, 2$  refer to the top and bottom elements of the composite beam. The missing parameters can be obtained from Figure 2.1.

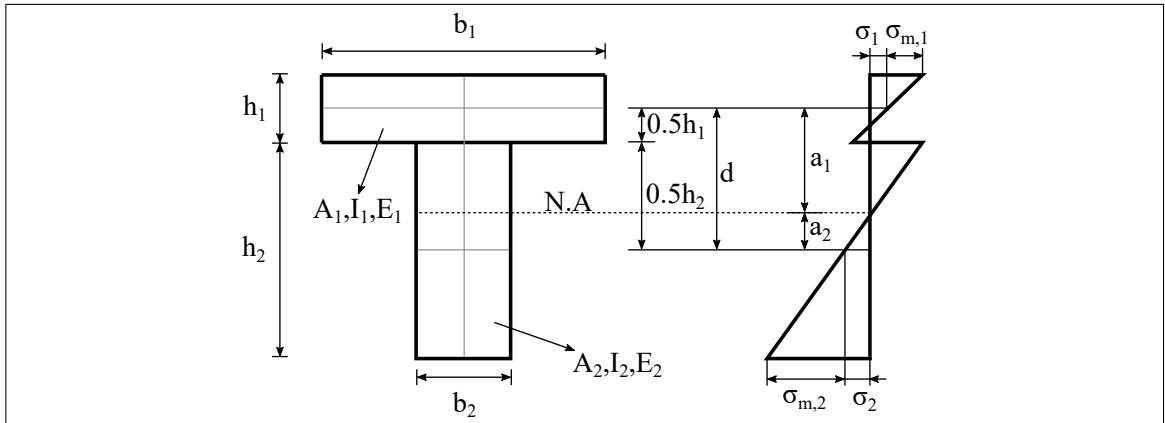


Figure 2.1. Cross section (left) and stress distribution (right) of a TCC.

When the beam is subjected to support conditions different of simply supported, the Eurocode 5 recommends a length of  $0.8L$  for continuous beams, and  $2L$  for cantilever beams. However, this assumptions may lead to errors of up to 27% in the prediction

of the maximum deflection (Girhammar, 2009), so this method is not recommended for boundary conditions different than simply supported.

## 2.2. Girhammar method

Girhammar (2009) proposed a simplified general method for analyzing and designing composite beams with interlayer slip, which can be applied to arbitrary boundary or loading conditions. The method is based on the theory for partial interaction beams with linear elastic conditions (Girhammar & Pan, 2007), and it was proposed as a simplification of the exact static analysis of composite beams, obtaining a method suitable for designing.

The method assumes that the mechanical fasteners with a constant shear flow stiffness,  $K = \frac{k}{s} \left[ \frac{N}{mm^2} \right]$ , where  $k$  is the slip stiffness and  $s$  the spacing of the fasteners, are equally spaced, and the frictional effects and uplift are neglected. Linear-elastic behavior is considered for all the component materials, and the curvature of the different components of the beam is assumed to be the same. Besides, the model considers the effective beam length equal to the buckling length of the equivalent buckling problem.

An effective bending stiffness was introduced in the model in order to reflect the effect of the interlayer slip and effective length. The effective bending stiffness depends of the geometrical properties of the sub-components, the slip modulus of the connection and the boundary conditions, as it can be seen in Equations 2.6 to 2.11.

$$EI_{eff} = \left[ 1 + \frac{\frac{EI_{\infty}}{EI_0} - 1}{1 + \left(\frac{\mu}{\pi}\right)^2 (\alpha L)^2} \right]^{-1} EI_{\infty} \quad (2.6)$$

$$\alpha = \sqrt{\frac{Kd^2}{EI_0 \left(1 - \frac{EI_0}{EI_{\infty}}\right)}} \quad (2.7)$$

$$EI_0 = E_1 I_1 + E_2 I_2 \quad (2.8)$$

$$EA_0 = E_1A_1 + E_2A_2 \quad (2.9)$$

$$EA_p = E_1A_1 \cdot E_2A_2 \quad (2.10)$$

$$EI_\infty = EI_0 + \frac{EA_p d^2}{EA_0} \quad (2.11)$$

where  $E_i I_i$ ,  $EI_0$  and  $EI_\infty$  are the bending stiffness of the sub component  $i$ , the bending stiffness of the non composite section and the bending stiffness of the fully composite section respectively. The boundary conditions depend on the buckling length coefficient,  $\mu$ , which is available in engineering handbooks (Girhammar, 2009). The missing parameters can be obtained from Figure 2.1.

In order to obtain the deflection of a composite beam for different boundary conditions, the bending stiffness of the fully composite section has to be replaced by the effective stiffness of the composite section (Equation 2.6). The procedure mentioned can be observed in Figure 2.2. It should be mentioned that both the  $\gamma$ - method and the Girhammar method give the exact same result when a simply supported beam is considered.

In addition to the deflection, the designers are usually interested in obtaining the internal forces. Knowing the force diagrams of a fully composite member, the internal forces can be approximated using the following expressions:

$$N_{i,eff} = \pm \left( 1 - \frac{EI_0}{EI_{eff}} \right) \frac{M}{d} \quad (2.12)$$

$$M_{i,eff} = \frac{E_i I_i}{EI_{eff}} M \quad (2.13)$$

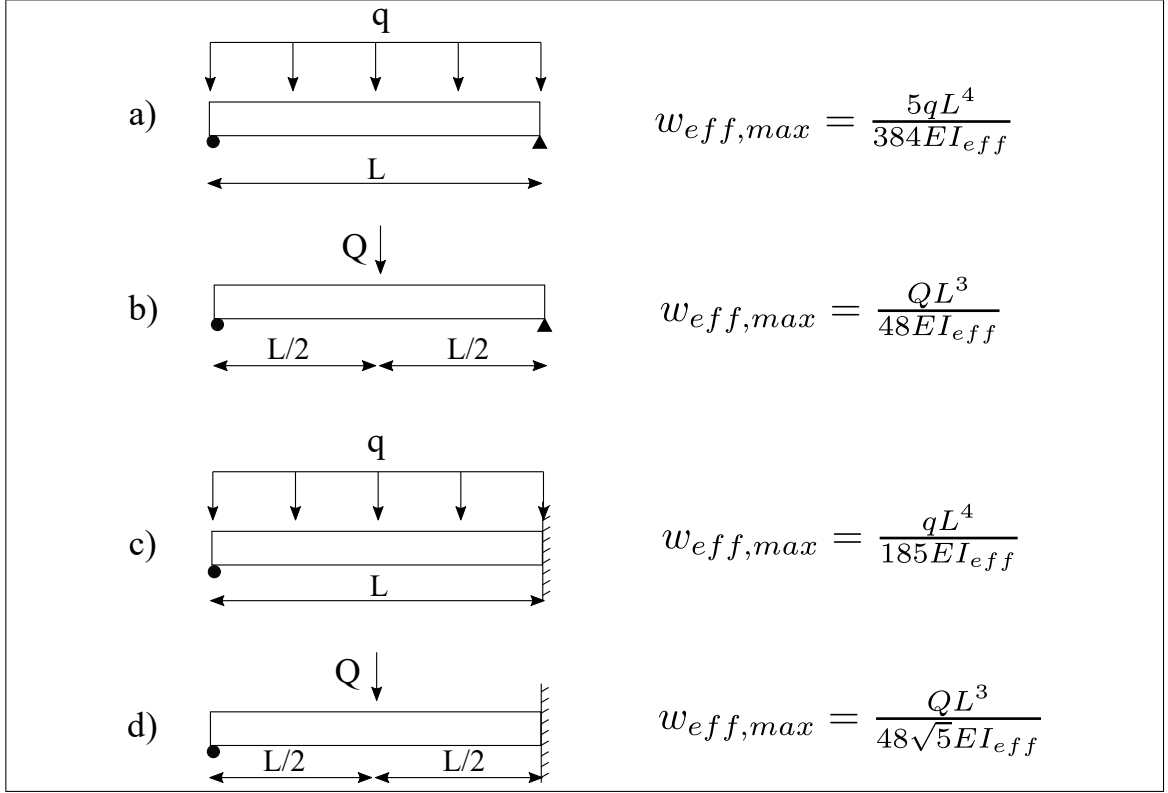


Figure 2.2. Approximate deflection expressions for beams with different loads and boundary conditions.

$$F_{s,eff} = \left(1 - \frac{EI_0}{EI_{eff}}\right) \frac{Vs}{d} \quad (2.14)$$

where  $M$ ,  $V$ ,  $N_{i,eff}$ ,  $M_{i,eff}$  and  $F_{s,eff}$  are the moment, shear, the normal force in the  $i$  component, moment in the  $i$  component and the load in the fasteners respectively, while  $i = 1, 2$  according to the Figure 2.1. On the other hand, the maximum normal and maximum shear stresses in the  $i$  sub component,  $\sigma_{i,eff,max}$  and  $\tau_{i,eff,max}$ , for rectangular sections, can be written as:

$$\sigma_{i,eff,max} = \sigma_i \mp \sigma_{i,b} = \left[ \left(1 - \frac{EI_0}{EI_{eff}}\right) \frac{1}{A_i d} \mp \frac{E_i h_i}{2EI_{eff}} \right] M \quad (2.15)$$

$$\tau_{i,eff,max} = \frac{E_i h_{na,i,eff}^2}{2EI_{eff}} V \quad (2.16)$$

where  $\sigma_i$  is the normal stress of the  $i$  component,  $\sigma_{i,b}$  is the bending stress of the  $i$  component and

$$h_{na,i,eff} = \min \left\{ \begin{array}{l} h_i \\ \frac{h_i}{2} + \left(1 - \frac{EI_0}{EI_{eff}}\right) \frac{EI_{eff}}{E_i A_i d} \end{array} \right. \quad (2.17)$$

### 2.3. Long-term simplified model

The aim of this section is to explain the analytical proposal to calculate the long-term deflection and stresses of the slab. The model was based on the proposal by Fragiaco (2006) to calculate long-term deflections, method that only considers simply supported conditions.

According to the numerical procedure proposed by Fragiaco (2006), the long term solution of the TCCs can be obtained by superimposing the effects of the loads, concrete shrinkage and inelastic strains due to environmental variations. A difficulty is, that the actual environmental conditions to which the TCC will be subjected are usually unknown. In this investigation, the relative humidity will be considered constant during its lifetime, and the daily and yearly temperature variations will not be considered.

The effects due to live and dead load for the simply supported case are usually evaluated through the "γ - method", formula widely employed in timber engineering. However, the same effects will be evaluated through the "Girhammar method" for other boundary conditions.

The effects of creep and mechanosorptive creep are considered by using the effective modulus method (Fragiaco, 2006), as described in the following equations:

$$E_{c,eff}^i = \frac{E_c(t_i)}{1 + \Phi_c(t, t_i)} \quad (2.18)$$

$$E_{w,eff}^i = \frac{E_w(t_i)}{1 + \Phi_w(t, t_i)} \quad (2.19)$$

$$k_{f,eff}^i = \frac{k_f(t_i)}{1 + \Phi_f(t, t_i)} \quad (2.20)$$

where  $\Phi_c(t, t_i)$  accounts for the creep phenomena in concrete,  $\Phi_w(t, t_i)$  accounts for the creep and mechanosorptive creep of the timber, and  $\Phi_f(t, t_i)$  is the creep coefficient of the connection.

To explain how to consider all the effects mentioned above,  $S$  represents a generic effect (mid-span deflection, slip, internal forces) at the time  $t$  from the cast of the concrete. In conformity with the superposition principle, the effect can be expressed as

$$S = S_h^{D+L} + S_h^s + S_{el}^y + S_{el}^d \quad (2.21)$$

where the subscripts  $el$  and  $h$  denote the type of analysis applied, elastic or hydroviscoelastic, and the superscripts denote load conditions, where  $D$ ,  $L$ ,  $s$ ,  $y$  and  $d$  symbolize the Dead Load, Live Load, concrete shrinkage, yearly inelastic strains due to thermohygro-metric variations and daily inelastic strains due to thermohygro-metric variations, respectively. As mentioned before, daily and yearly temperature variations will not be considered in this model, so the last component of equation 2.21 can be disregarded, while  $S_{el}^y$  can be considered as yearly inelastic strains due to hygrometric variations.

$$S = S_h^{D+L} + S_h^s + S_{el}^y \quad (2.22)$$

In order to determine the effect of the Dead and Live loads, it will be considered the following:

$$S_h^{D+L} = S_h^D + S_h^L \quad (2.23)$$

$$S_h^i = F_{el}^i(E_{c,eff}^i, E_{w,eff}^i, k_{f,eff}^i) \quad \text{with } i = D, L \quad (2.24)$$

where  $F_{el}^i$  is the load  $i$  evaluated with the  $\gamma$ -method or Girhammar method, depending of the boundary conditions, by replacing the effective modulus as it is seen in equations 2.18, 2.19 and 2.20. In order to be consistent with the considerations of Fragiaco (2006), the CEB 90 (1993) will be used to calculate the creep coefficient of the concrete.

The effect of the concrete shrinkage in the TCC is considered as

$$S_h^s = F_{el}^{\Delta\varepsilon_{sh}}(E_{c,eff}^s, E_{w,eff}^s, k_{f,eff}^s) \quad (2.25)$$

where  $F_{el}^{\Delta\varepsilon_{sh}}$  is calculated by solving the differential equation of TCCs, which solution is given by Fragiaco (2006) for a simply supported beam. The solution of the differential equation for boundary conditions different to simply supported is reported in Appendix A. The inelastic strain,  $\Delta\varepsilon_{sh}$ , will be estimated by following the expressions proposed in CEB 90 (1993).

The Toratti model (1993) was used to define the timber and connection creep modulus. This model can predict the creep of timber in varying environment humidity, when subjected to bending, tension or compression parallel to the grain (Toratti, 1993). It considers a piecewise linear moisture content history which varies  $\Delta u$  in a period  $\Delta t = 365$  days. The model can be described as

$$\begin{aligned}
\Phi_w(t, \tau) &= \Phi_{wc}(t - \tau) + \Phi_{wms}(t - \tau) \\
&= \frac{E_w(u)}{E_w(u_{ref})} \left( \frac{t - \tau}{t_d} \right)^m + \frac{0.7E_w(u)}{E_w(u_{ref})} [1 - e^{-c_w(2\Delta u/\Delta t)(t-\tau)}]
\end{aligned} \tag{2.26}$$

where  $\Phi_{wc}$  is the creep part and  $\Phi_{wms}$  is the mechanosorptive part of the total creep coefficient  $\Phi_w$ ,  $\tau$  is the current time,  $t$  the time at which creep starts (usually when the load is applied),  $u_{ref} = 0.2$ ,  $c_w = 2.5$ ,  $t_d = 29500$  days and  $m = 0.21$  (Fragiacomo & Ceccotti, 2006b).

Figure 2.3 shows a comparison of the timber creep coefficient variation over the years, considering different values of moisture content defined in terms of  $\Delta u$ . It can be observed that after 50 years the value of the timber creep coefficient  $\Phi_w$  is independent of the amplitudes of the moisture for values of  $\Delta u$  larger than 1.65%, which is typical of TCCs (Fragiacomo & Ceccotti, 2006b). For this reason, and since it is the average timber moisture content measured by Fragiaco (2006) for a real TCC beam, the value of  $\Delta u$  considered for this thesis is  $\Delta u = 3.3\%$ .

Because the variation of the timber elastic modulus due to moisture is usually insignificant, the equation 2.26 can be simplified by considering  $E_w(u) = E_w(u_{ref}) = E_w$  (Fragiacomo, 2006). In absence of experimental tests of the long-term behavior of the connection, the recommendation of the EC5 (1995) is to use  $k_f = 2\Phi_w$ .

## 2.4. Finite Element Modeling

In order to compare and validate the analytical models, finite element models were developed using the software ANSYS. Three models were developed for this purpose: a two dimensional linear model called FEM 2D, a three dimensional linear model called FEM 3D L, and a three dimensional non linear model called FEM 3D NL. In this section, it can be found an explanation of the material properties, adopted elements, constitutive

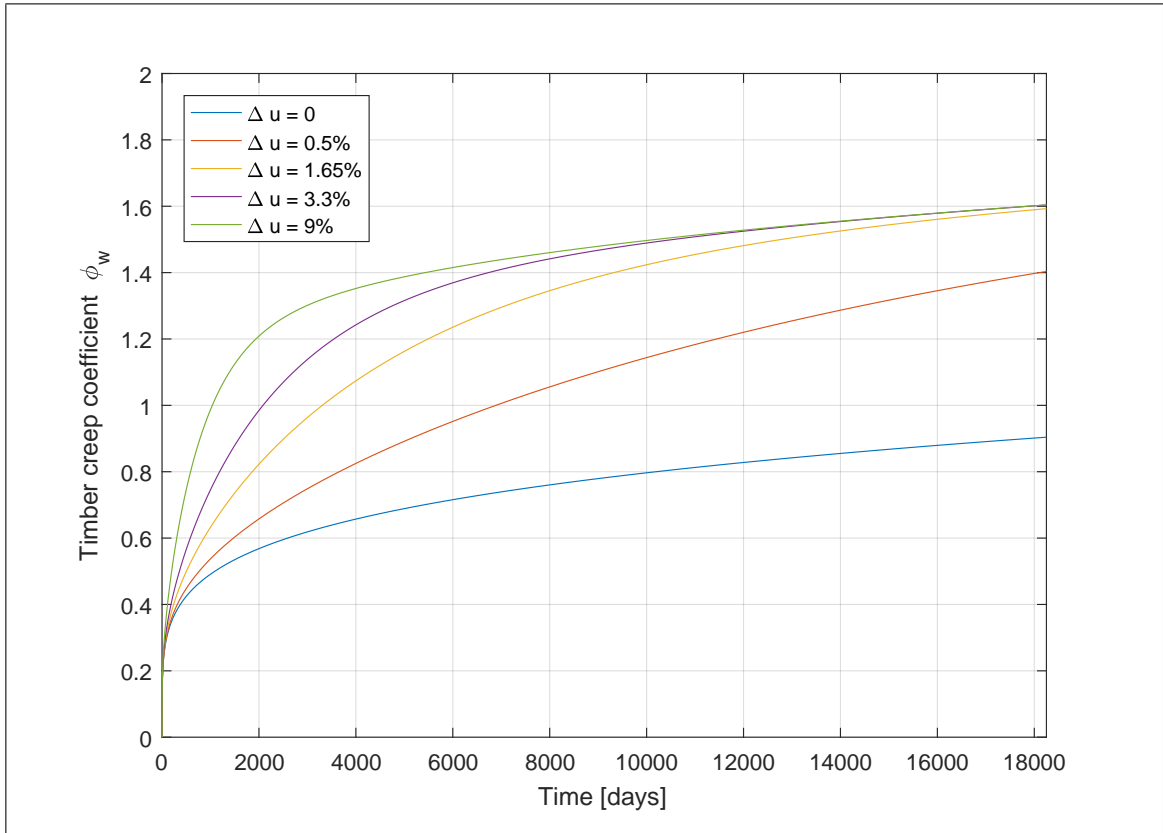


Figure 2.3. Creep coefficients of timber considering different values of  $\Delta u$ .

relations and assumptions made to develop the models, including the short-term and long-term behavior.

#### 2.4.1. Elements used

For the two dimensional linear model, the element PLANE183 was used for the short-term and long-term behavior of the concrete and timber. This is an eight node element (Quad) with two degrees of freedom at each node: translations in the  $x$  and  $y$  directions.

For the three dimensional linear model, the element SOLID186 was used for modeling of the concrete and timber. The element has twenty nodes with three degrees of freedom at each node: translations in the  $x$ ,  $y$  and  $z$  directions. The element exhibit quadratic displacement behavior and isotropic modules were considered for both materials.

The three dimensional element SOLID65 was used for the purpose of modeling the non linear behavior of the concrete. When the concrete material model is included, the element can consider the presence of reinforcing bars and is capable of cracking in tension and crushing in compression. The steel reinforcement was modeled with an uniaxial tension-compression element, LINK180, considering an elastic-perfectly plastic constitutive relation.

An isotropic module was considered for modeling the timber in the non-linear model, since when the behavior is flexure dominated and the timber is free of defects, the influence of the properties in the direction perpendicular to the grain is negligible (Khorsandnia et al., 2014). The element SOLID185 was used to model the timber, which is an eight node element with three degrees of freedom at each node.

#### **2.4.2. Connection system**

The connection system is modeled by discrete longitudinal springs which connect the upper component of the beam (concrete) with the lower component (timber). The model does not consider the local effects caused by the connectors, since the objective of the model is to observe the global behavior of the beam.

The joint between the timber and concrete section was modeled with COMBIN14 spring elements. Several authors have used spring elements at the position of the shear connectors, to model mechanical fasteners (Fragiacomo et al., 2007; Lukaszewska et al., 2010; Lopes, Jorge, & Cruz, 2012) or notches, screws and continuous connections (Khorsandnia et al., 2014). Since the connection strength is designed to be larger than the shear force in the connectors, a linear behavior is expected, and therefore, the connection was modeled as linear with a slip modulus  $k_s = \frac{K}{s}$ .

### 2.4.3. Concrete shrinkage

As it was mentioned in Section 1.4.3, the effect of the concrete shrinkage is quite important in TCCs. In order to measure its effect, and in absence of the solution for boundary conditions different to simply supported in the bibliography, the differential equation of the TCC was solved and its solution is reported in Appendix A.

In the absence of the option of considering the concrete shrinkage in ANSYS, the effect was introduced by applying a fictitious change of temperature which induces the same value of strain in the concrete as free shrinkage does. The concrete coefficient of thermal expansion was considered as  $\alpha = 1.4E - 04 \frac{1}{\circ C}$ , which is the default concrete value in Ansys. Then, the time dependent temperature,  $T(t)$ , was calculated as

$$T(t) = \frac{\varepsilon_{sh}(t)}{\alpha} \quad (2.27)$$

where  $\varepsilon_{sh}(t)$  is the free shrinkage strain calculated with the CEB 90 shrinkage model (1993).

Figure 2.4 shows a comparison of the deflection induced by shrinkage for a simply supported beam and a propped cantilever beam obtained using the FEM 3D L. The prediction of the analytical method reported in Appendix A was plotted as a comparison. It can be observed an almost perfect agreement between the two models, regardless the boundary conditions.

### 2.4.4. Creep

For the long term behavior, creep effects were considered in the concrete and timber. As mentioned in Section 2.3, CEB 90 (1993) Model code and Toratti model (1993) were considered as creep models for concrete and timber respectively. However, ANSYS has their own creep equations for modeling the behavior of the materials, with constants that can be adjusted in order to fit the target model.

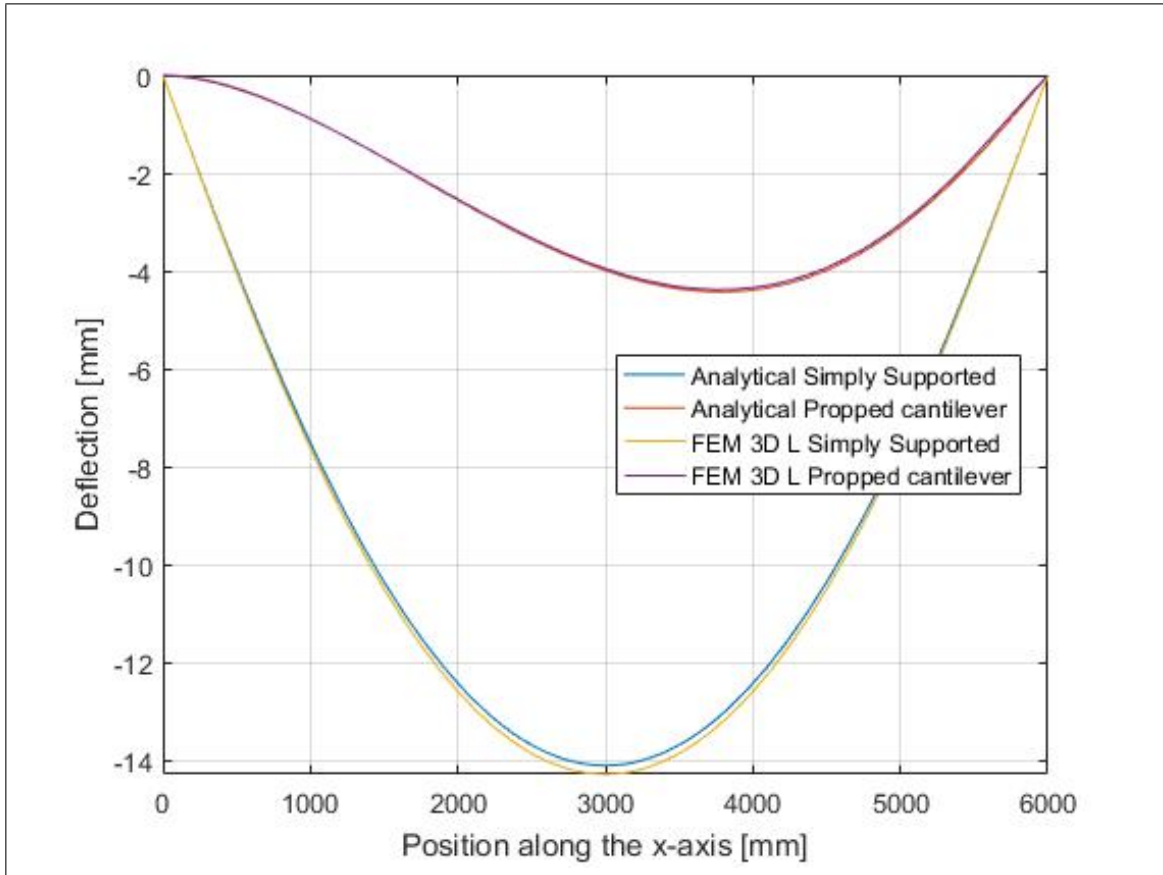


Figure 2.4. Deflections in five years induced by concrete shrinkage for different support conditions.

Since the CEB 90 (1993) and Toratti (1993) models are functions of time, the model "Modified Time Hardening" available in ANSYS was found to be the best option for representing the creep models. The ANSYS model can be observed in Equation 2.28, where  $C_1$ ,  $C_2$ ,  $C_3$  and  $C_4$  are constants,  $T$  is the temperature of the material,  $t$  is the current time,  $\sigma$  is the material stress and  $\varepsilon_{cr}$  is the creep strain.

$$\varepsilon_{cr} = \frac{C_1 \sigma C_2 t^{C_3+1} e^{-\frac{C_4}{T}}}{C_3 + 1} \quad (2.28)$$

As it can be seen in Equation 2.28, creep strain is dependent of the stress of the material, which during the analysis remains constant while the creep strain increases with a time dependent rate. A comparison between the adjusted ANSYS models and the CEB

90 (1993) or Toratti (1993) model can be observed in Figure B.1 and B.2 for a five years period, and in Figures B.3 and B.4 for a fifty years period. The constants  $C_1$ ,  $C_2$ ,  $C_3$  and  $C_4$  adjusted for each figure are shown in Table B.1, B.2 , B.3 and B.4 respectively.

### 3. NUMERICAL AND EXPERIMENTAL VALIDATION

The objective of this section is to validate the analytical models presented in Chapter 2, using the Finite Element method by analyzing a slab designed in cooperation with a Chilean company, ISiete, since they were interested in including a TCC slab in a residential building.

#### 3.1. Section Design and Material Properties

In order to analyze a slab designed as real as possible, several restrictions were considered during the design process, which include geometrical, economical and code limitations:

- The length of the slab shall be 6000 mm, considering that it is the largest slab length in a typical residential building.
- The total depth of the slab shall be smaller than 170 mm, since larger depths are not competitive with a traditional concrete slab, especially for mid and high rise concrete buildings, where the space of one or more entire stories may be lost when considering thicker slabs
- The concrete layer shall be thicker than 70 mm, since all the electrical conduits and installations in the slab must be accommodated through inside the concrete.
- In absence of design regulations for TCCs, the deflection limits shall fulfill the requirements of ACI318-14 (2014).

Considering the restrictions mentioned, a section of the final design can be observed in Figure 3.1. The timber considered in this design is Laminated Strand Lumber (LSL).

Regarding the material properties, the concrete resistance was considered as  $f'_c = 41$  MPa, the timber elastic modulus as  $E_w = 12065$  MPa (Louisiana Pacific Corporation, 2019), the slip modulus of the connection  $K_s = 20 \frac{kN}{mm}$  (Rothoblaas, n.d.) with a spacing of  $s = 200$  mm. The concrete elastic modulus and tensile strength were obtained by using

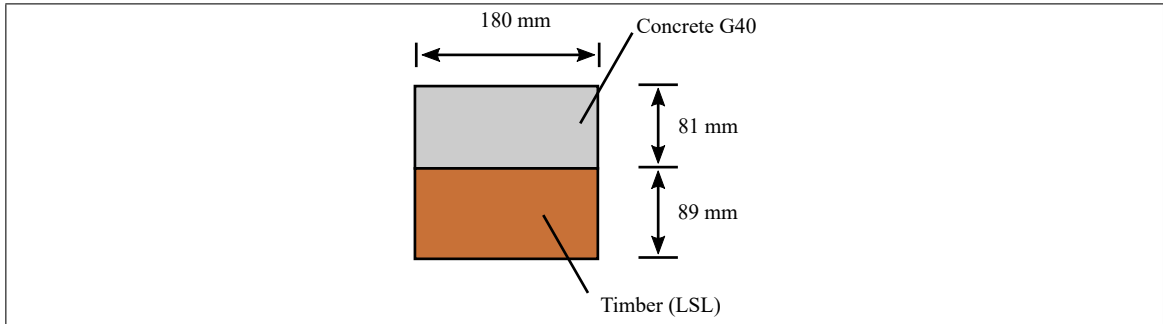


Figure 3.1. Slab design.

$E_c = 4700\sqrt{f'_c}$  and  $f_t = 0.62\sqrt{f'_c}$  respectively (American Concrete Institute, 2014). The concrete reinforcement considered for the areas with negative moment in the FEM 3D NL model were 8-mm bars spaced at 60 mm, with a yield stress of 420 MPa, simulating a real reinforcement.

### 3.2. Short term behavior

For the short term behavior, two methods were used to analyze the performance of the beam: analytical and FEM. Since the support conditions of the beam are different to simply supported, the most adequate analytical model is the Girhammar Method (Section 2.2). Table 3.1 shows a comparison of the maximum deflections predicted by the FEM 2D model and the Girhammar method (Analytical) model, for different boundary conditions and subjected to service loads. As it can be observed in the table, the Analytical model can accurately predict the maximum deflection regardless of the support conditions.

Table 3.1. Maximum deflection comparison under different support conditions for service loads.

Model	Simply Supported [mm]	Propped cantilever [mm]	Fixed [mm]
Analytical	15.35	7.56	4.42
FEM 2D	15.45	7.87	4.42
%Error	0.67%	3.94%	0.04 %

The service loads were chosen according to the Chilean code specification, NCh1537.Of2009, which defines the minimum values to be considered for the service and permanent loads (Instituto Nacional de Normalización, 2009). Considering that the loads have to be consistent with the solicitation of a residential building, the values selected were:

- Dead Load :  $D = 0.981 \text{ kPa}$
- Live Load :  $L = 1.962 \text{ kPa}$

With the loads defined, the first step to validate the analytical model is to compare the deflections. This indicator is directly related to the stiffness of the TCC and the support conditions, reason why it is a very important one. Besides, as it was mentioned in Section 1.4, the deflection is often the indicator which controls the design. The results are presented in Table 3.2.

Table 3.2. Instantaneous deflection for a propped cantilever beam subjected to service loads.

Model	Max deflection [mm]
Analytical	7.56
FEM 2D	7.77
FEM 3D L	7.60
FEM 3D NL	8.62

As it can be observed in Table 3.2, the analytical model gives a close prediction compared to the FEM 2D and FEM 3D L model. However, when comparing the analytical model with the FEM 3D NL model, the analytical result is 13.3 % smaller than the FEM 3D NL prediction. This result was expected since the analytical model does not consider the cracking of the concrete, as the FEM 3D NL does.

In addition to the deflections, to fully validate the analytical model all the design parameters were checked. In other words, the model has to give a reasonable accurate prediction of the concrete and timber stresses, and interface forces. The main stresses of the timber and concrete were calculated and are presented in Table 3.3. The table is divided in two sections, in order to observe the main stresses at mid-span and at the fixed support.

Table 3.3. Stresses for a propped cantilever beam subjected to service loads.

Mid-span		
Model	Concrete compression [MPa]	Timber tension [MPa]
Analytical	4.55	2.58
FEM 2D	4.64	2.64
FEM 3D L	4.95	2.65
FEM 3D NL	4.72	2.50
Fixed end		
Model	Concrete tension [MPa]	Timber compression [MPa]
Analytical	8.09	7.56
FEM 2D	10.6	5.84
FEM 3D L	10.9	6.78
FEM 3D NL	3.36	8.95

Analyzing the mid-span stresses, it can be observed a good agreement between the Analytical model and all the numerical ones. The largest difference occurs between the Analytical model and the FEM 3D L model, yet the difference is less than 8.1%. However, it is expected that the prediction of the FEM 3D NL will be closer to the real case, since it accounts for the concrete non linear behavior, yet the difference with the Analytical model in the prediction of the stresses is near 3.6%.

On the other hand, larger differences are observed in the fixed end case. Regarding the concrete tensile stresses, the results of the linear models are not expected to be accurate since they do not consider cracking of the concrete, while the FEM 3D NL does. The analytical model underestimates the concrete tension compared to the linear numerical models, which are in good agreement between them and overestimates the concrete tension compared to the FEM 3D NL model by 140%. Regarding the timber compression stresses, all the models gave different results. The analytical model and the FEM 3D NL model are the larger stresses, being the analytical stresses 16 % smaller.

Table 3.4 shows a comparison of the interlayer forces obtained with the Analytical model and the Finite Element Models, at five points along the length of the slab. The interlayer force  $F_s$  at the fixed end ( $x = 0$ ) draws attention, given the contradictory results between the analytical and Finite Element Models. The explanation of this is that in order to obtain the exact interlayer force, the interlayer slip must be calculated ( $F_s = ks(x)$ ). Due to the complexity of the procedure, the Equation 2.14 was proposed by Girhammar (2009) as an approximation to estimate  $F_s$  as a function of the shear force. However, errors in the prediction of the interlayer force at the fixed end are expected since, even though it is known that the interlayer slip is 0, the shear force  $V$  is largest at this end so the Equation 2.14 provides a result different from 0.

When observing the interlayer forces along the length of the beam predicted by the analytical and numerical models, it can be concluded that both approaches are in good agreement with each other, since the maximum difference between them is less than 12 %. Comparing the Analytical model with the FEM 3D NL model, the maximum difference occurs near the fixed end ( $\frac{1}{4}L$ ) where the Analytical model overestimate the interlayer force by 12 %, while at three quarters of the length ( $\frac{3}{4}L$ ) the interlayer force is underestimated by 4 %.

Table 3.4. Interlayer force along the x axis for the different models.

Model	$F_s(0)$ [kN]	$F_s(\frac{1}{4}L)$ [kN]	$F_s(\frac{1}{2}L)$ [kN]	$F_s(\frac{3}{4}L)$ [kN]	$F_s(L)$ [kN]
Analytical	5.27	3.30	1.05	1.19	3.16
FEM 2D	0	3.20	1.16	1.10	3.07
FEM 3D L	0	2.99	1.12	1.35	2.85
FEM 3D NL	0	2.95	0.96	1.24	3.04

### 3.3. Long term behavior

In absence of long term experimental data of TCC beams or slabs subjected to boundary conditions different than simply supported, a numerical long-term model was made with ANSYS to compare with the analytical model proposed in Section 2.3.

The cross-section of the analyzed slab is shown in Figure 3.1, and the material properties were given in Section 3.1. Since the Live Load shall not be present during the entire life cycle of the slab, the load combination usually applied to obtain the long-term effects is  $D + 0.3L$ . The loads considered are equal to the ones mentioned in the previous section, and they were applied 21 days after the concrete casting, in order to simulate real conditions.

As mentioned in Section 2.3, the long-term behavior can be obtained by superimposing the effects of the loads, concrete shrinkage and inelastic strains due to hygrometric variations. A comparison of the maximum deflections calculated with the Analytical and FEM 2D models for a simply-supported slab can be seen in Figure 3.2 for a period of five years since concrete casting. The contribution of each effect is represented by the vertical arrows, being the concrete shrinkage the most influential effect over the long-term deflection.

The same analysis was performed by changing the support conditions to a propped cantilever slab, and the results are shown in Figure 3.3. As in Figure 3.2, the contribution

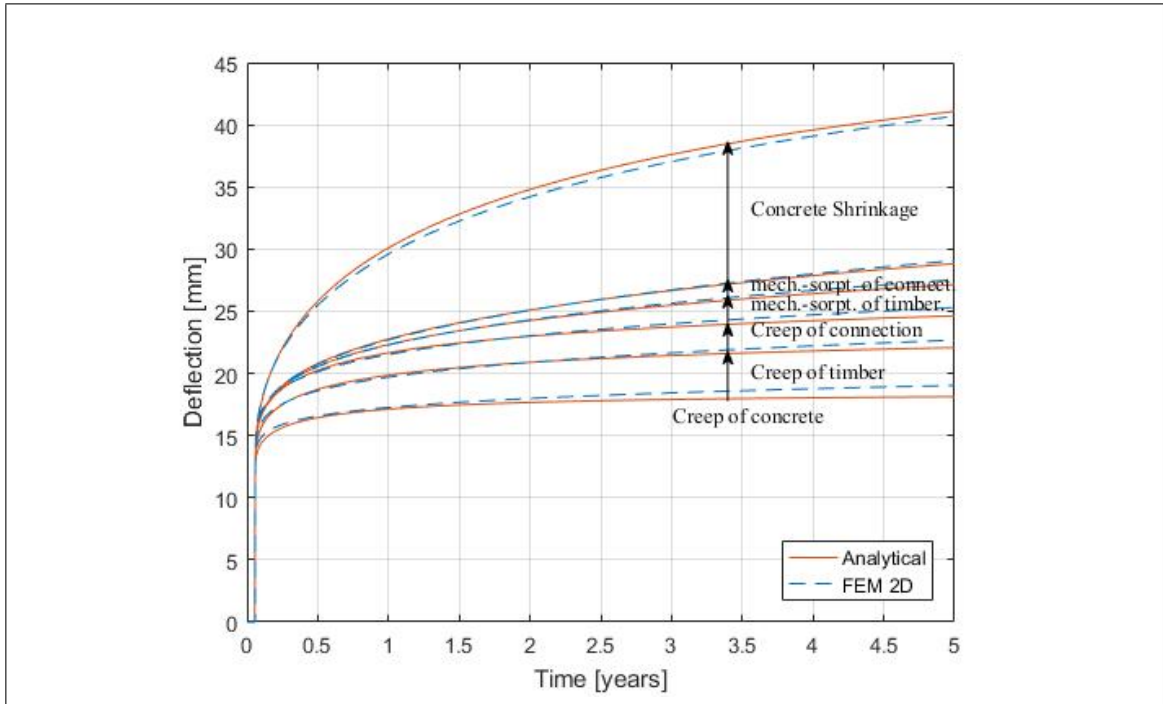


Figure 3.2. Simply supported beam long term maximum deflection at mid-span.

of each effect is represented by vertical arrows, being the concrete shrinkage the most influential effect over the long-term deflection. The maximum deflection predicted by the FEM 2D model was 19.24 mm, while the Analytical model predicted 18.27 mm of maximum deflection. This implies that the Analytical model prediction is very similar to the numerical one, underestimating the deflection for the propped cantilever condition by 5.1%. A comparison between the two different support conditions can be observed in Figure 3.4.

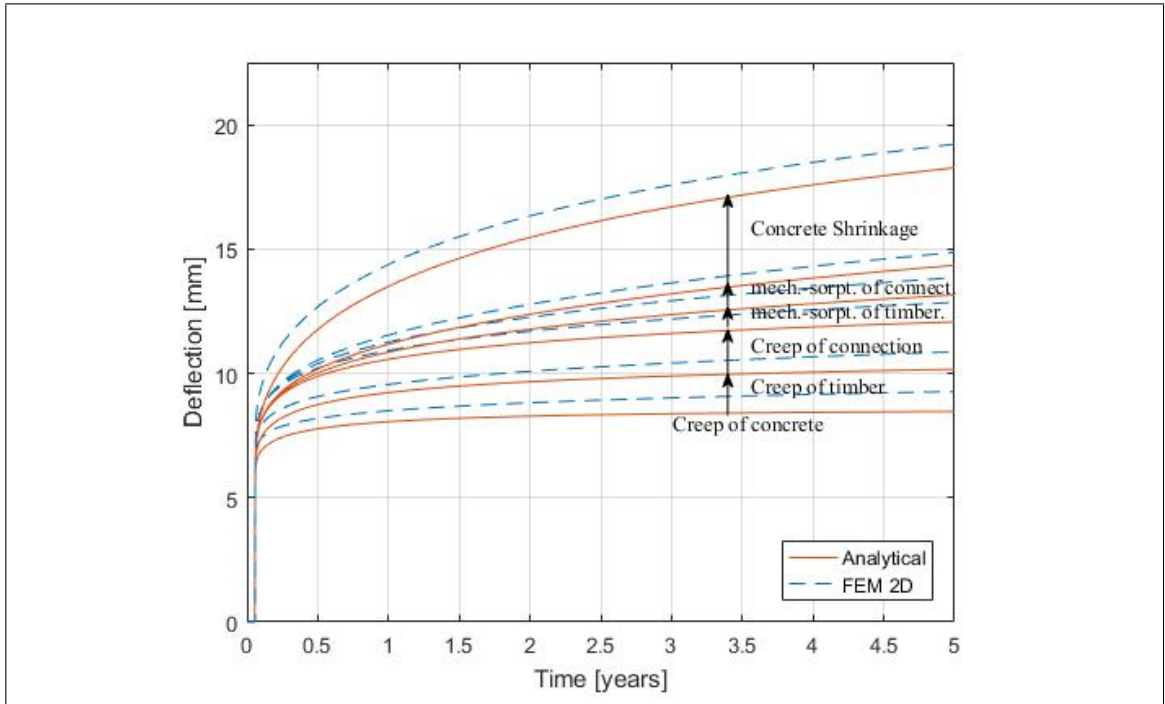


Figure 3.3. Propped cantilever beam long term maximum deflection.

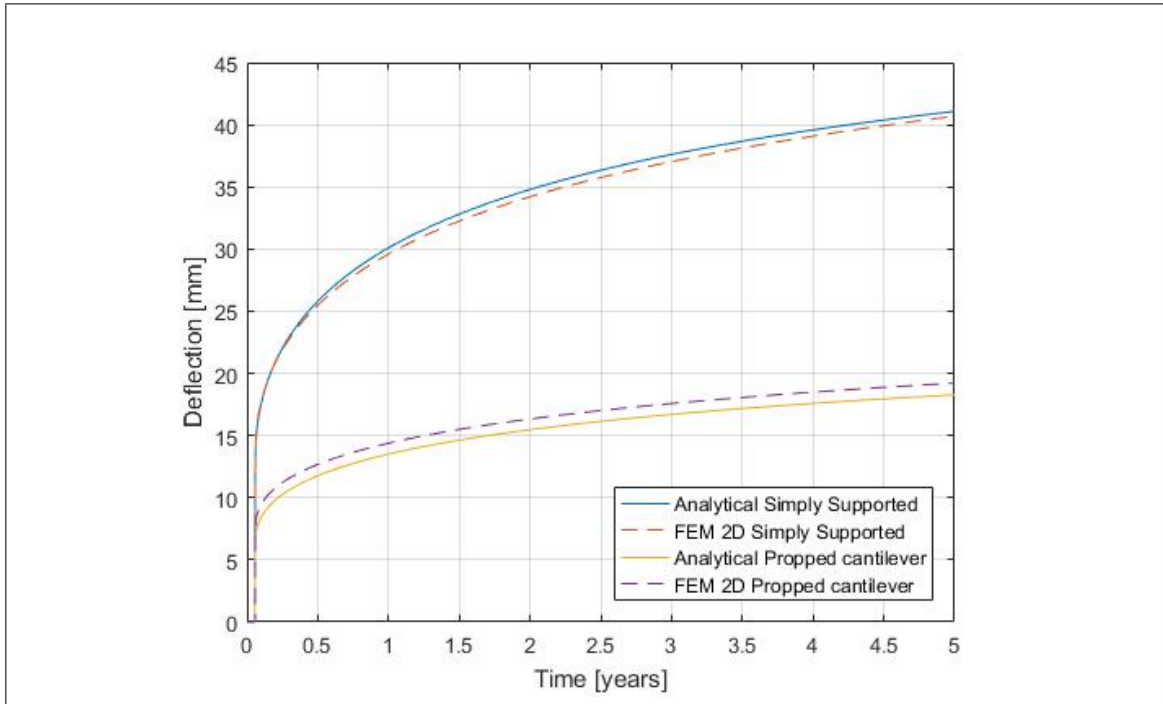


Figure 3.4. Long term deflection (5 years).

It can be observed from Figure 3.2 and Figure 3.3 that the analytical prediction is in good agreement with the numerical one, regardless the boundary conditions. The 5 years deflection is approximately 3 times the instant deflection for the simply supported case, and 2.6 times the instant deflection for the propped cantilever case. Additionally, it can be observed from Figure 3.4 that the maximum deflection of a propped cantilever slab at 5 years since concrete casting is at least 50% smaller than the maximum deflection of a simply-supported slab.

For a fifty years period since concrete casting, it was not possible to emulate in ANSYS the CEB 90 (1993) and Toratti (1993) creep model with precision, since neither the "Modified Time Hardening" or other models available in ANSYS fitted those models (see Figure B.3, B.4). Even so, the comparisons of the deflections calculated for fifty years since concrete casting were done and are shown in Figure 3.5.

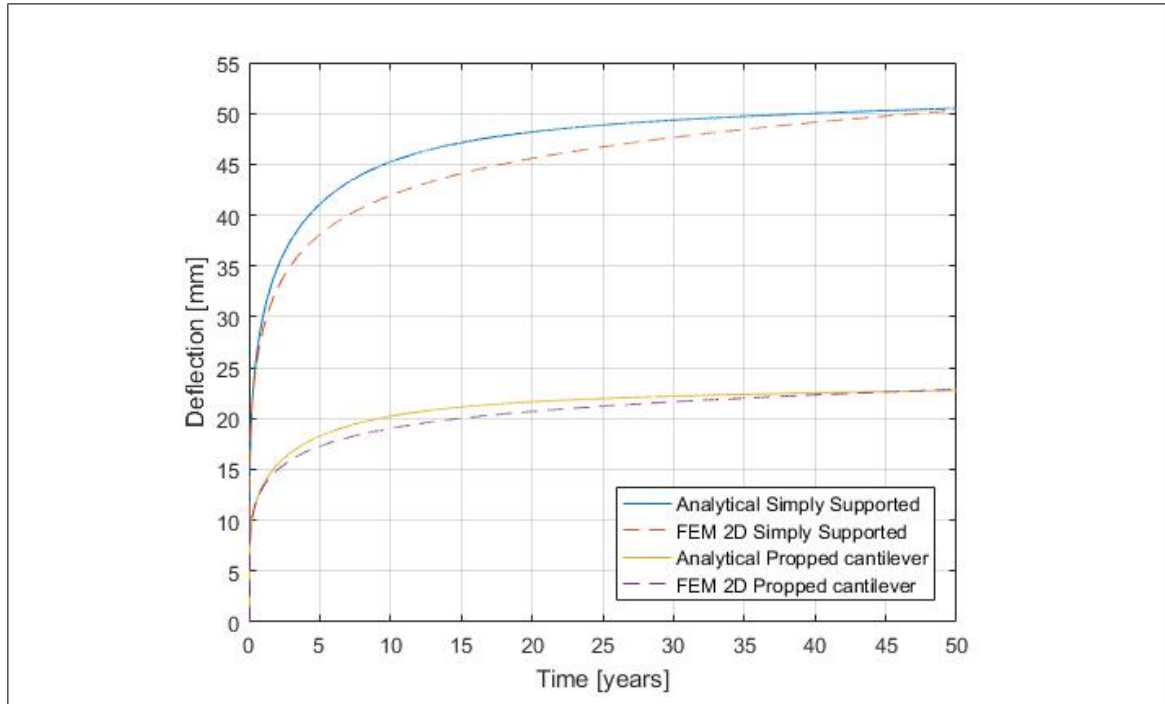


Figure 3.5. Long term deflection (50 years).

From Figure 3.5, it can be observed that the 50 years deflection is approximately 4 times the instant deflection for a simply supported beam, and 3.3 times the instant deflection for the propped cantilever case. Additionally, the maximum deflection of a propped cantilever slab at fifty years since concrete casting is at least 50% smaller than the maximum deflection of a simply-supported slab, as in the five years analysis. However, in 10 years up to 88% of the 50 years deflection developed for the simply supported case, while up to 85% developed for the propped cantilever case, consequently a 50 years analysis might not be necessary.

### 3.4. Experimental validation

For the purpose of experimental validation of the Girhammar method, the prediction of the analytical model was compared with the test results of Sebastian et al.(2016). The authors tested two propped cantilever TCC beams, to understand the behavior of external

indeterminacy in the longitudinal direction with presence of cracked concrete zones and changes in the connection behavior (Sebastian et al., 2016). The geometry of the beams can be observed in Figure 3.6.

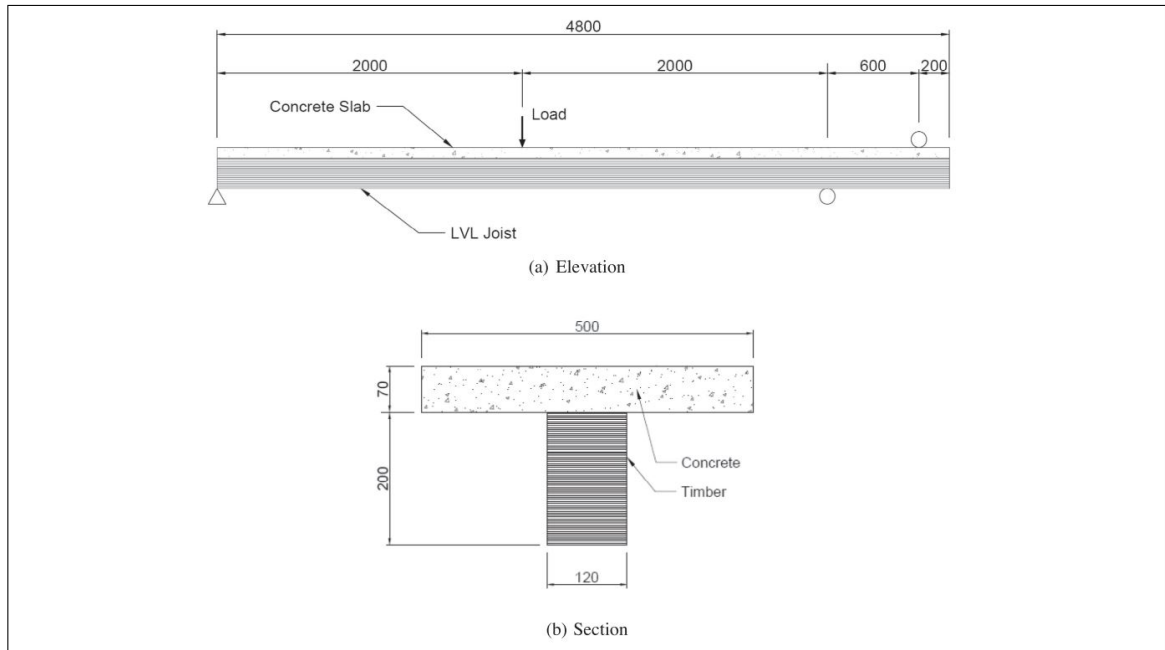


Figure 3.6. Dimensions [mm] of the TCC beam. (Sebastian et al.,2016).

In addition to the TCC bending tests, the concrete, timber and the connection were tested by Sebastian et. al. (2016) to obtain their properties. Partially Threaded Screws (PT) and Fully Threaded Screws (FT) were tested to obtain the slip modulus and the failure load of the connection. Tests were performed to obtain the connection behavior when the concrete is compressed (traditional test) and when the concrete develops tension stresses and eventually cracks (Sebastian et al., 2016). Only the results of the tests of the PT screws are shown in Table 3.6 since the beam modeled in this article used those connectors. More details of all the tests can be found in Sebastian et. al. (2016).

Table 3.5. Timber and concrete properties.

Concrete		Timber		Steel	
$E_c$ [GPa]	31.0	$E_w$ [GPa]	15.7	$E_s$ [GPa]	191.0
$f'_c$ [MPa]	32.7			$f_y$ [MPa]	354.0

Table 3.6. PT connection properties from tests.

Screw/Test	Failure load [kN]	Slip modulus [ $\frac{kN}{mm}$ ]
PT/compression	39.0	23.2
PT/tension	10.4	8.0

Three numerical models were used to estimate the short-term behavior of the slab. The first one, "Ansys L Fixed", consists of a 4 m beam perfectly fixed on one end, and simply supported at the other end. The timber and concrete were modeled as linear, and the dimensions of the cross section are shown in Figure 3.6 b). The second and third numerical models ("Ansys L" and "Ansys NL") correspond to full models of the beams, in an attempt to emulate the actual conditions of the tests with a linear and a non-linear behavior, since it was believed that the test set up did not emulate a perfect fixed support. In Figure 3.7 can be observed the geometry of these models, with text labels for better understanding.

A 35 mm thick steel plate connected to the floor by two  $\phi 28$  steel bars, was used to restrain the uplift of the cantilever end of the beam. Another 35 mm thick steel plate was used to distribute the applied load, and 50 mm thick steel plates were used to model the supports. The behavior of the concrete was considered linear in the Ansys L model and non-linear in the Ansys NL model, while the behavior of the timber was considered linear in both cases. Regarding the analytical model, the Girhammar method was used to predict

the short-term behavior of the beam, as described in Section 2.2. The beam was modeled as a 4m element, simply supported in one end and perfectly fixed at the other end.

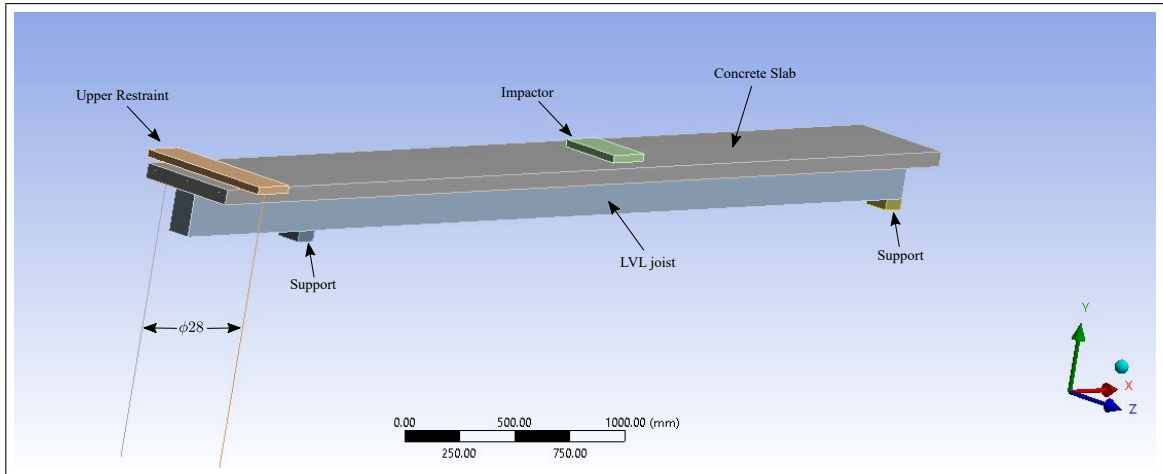


Figure 3.7. Ansys NL and Ansys L model. Images used courtesy of ANSYS,inc.

Both connection slip modulus were used in the numerical models, using the tension slip modulus for the zone near the fixed support, where the concrete develops tension, and the compression slip modulus for the rest of the beam. On the other hand, since the analytical model can only consider one slip modulus, one model was done with each connection. A summary of the models is presented in Table 3.7. It is important to mention that linear behavior of the connectors was considered for the analytical and numerical models, since the peak forces measured during the test of the beam were still on the linear portion of the behavior of the connection (Sebastian et al., 2016).

Table 3.7 shows that the Ansys NL model is the one which better represents the actual conditions of the test, since it considers the upper restraint and the non-linear behavior of the concrete. The Ansys L model does represent the support conditions of the test, but it does not consider the real behavior of the materials since linear behavior of concrete is considered, while the Ansys L Fixed model simplifies the conditions at the fixed support considering a perfectly fixed support. Lastly, the analytical models consider a perfectly fixed support, and does not account the variation of the connectors slip stiffness along the beam.

Table 3.7. Summary of the models.

Model	Model Type	Fixed Support	Connection Slip Modulus	Concrete behavior
Analytical 8 kN/mm	Analytical	Perfectly fixed	Tension	Linear
Analytical 23 kN/mm	Analytical	Perfectly fixed	Compression	Linear
Ansys L Fixed	Numerical	Perfectly fixed	Both	Linear
Ansys L	Numerical	Test Setup	Both	Linear
Ansys NL	Numerical	Test Setup	Both	Non Linear

In Figure 3.8 can be observed a comparison of the load-deflection response obtained with the models from Table 3.7 and the test results, which were adapted from Sebastian et al.(2016). Regarding the test results, the response of the beam is approximately linear until 140 kN, when longitudinal cracks appeared in the concrete, leading to a sharp drop of stiffness (Sebastian et al., 2016). The Ansys NL model is in very close agreement with the test results after the 40 kN load. In addition, 2.22 mm uplift of the Upper Restraint (see Figure 3.7) was calculated in the Ansys NL model at 120 kN load. All this together suggests that the test setup did not provide a perfectly fixed support.

As expected, the linear Ansys L model is stiffer than the non linear one, and the difference between the two models is less than 9% for loads smaller than 140 kN. The Ansys L model underestimates by 16 % the deflection of the test at 120 kN load.

As it is shown in Table 3.7, the difference between the Ansys L and the Ansys L Fixed model is the configuration of the fixed support: while the Ansys L model emulates the test configuration, the Ansys L Fixed model has one of its ends perfectly fixed. That consideration led the Ansys L Fixed model to be the stiffest numerical model and to underestimate the experimental deflection by 23 % for a 120 kN load.

Among all the models, the analytical model which considers the largest slip modulus is the stiffest of all models. This occurs because the model assumes a perfectly fixed end, and also the largest possible connection slip modulus. On the other hand, the Analytical 8

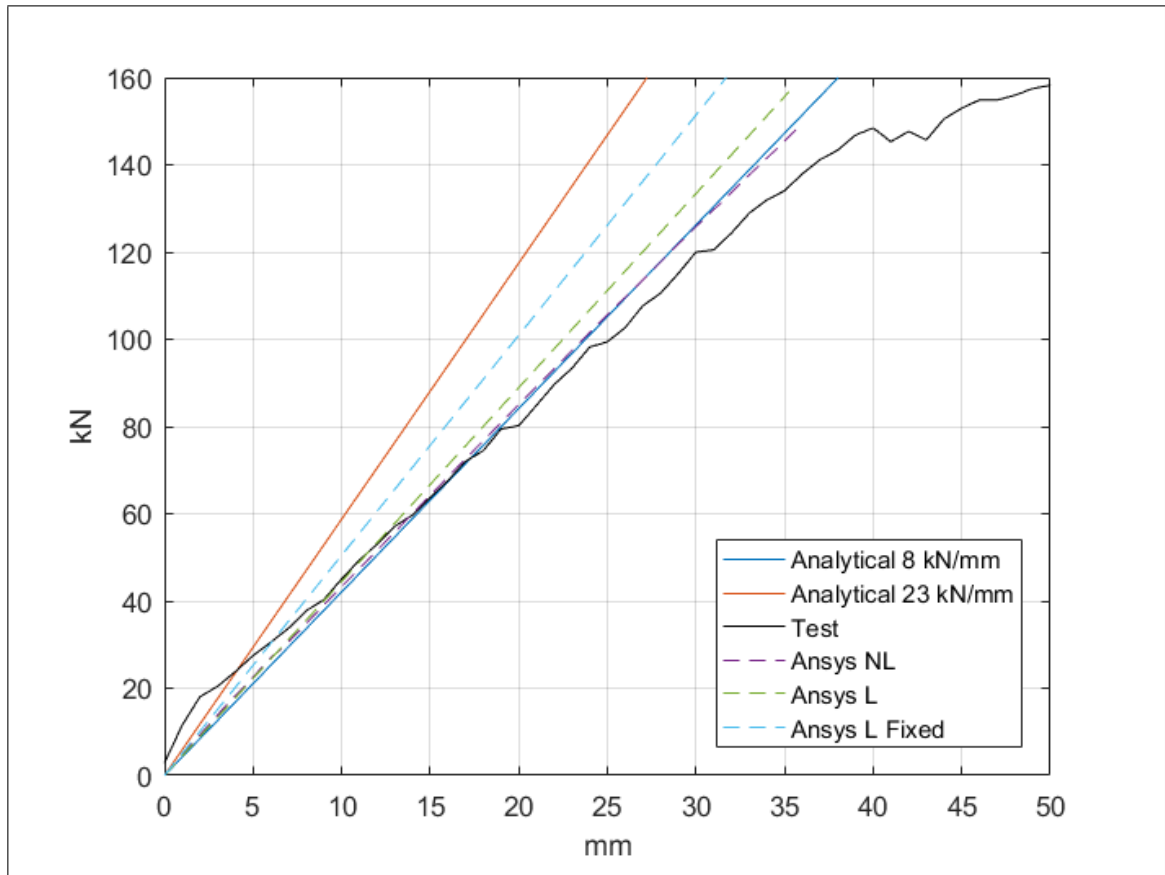


Figure 3.8. Deflection of the PT beam. Test results adapted from Sebastian et al. (2016).

kN/mm model is more flexible than the Analytical 23 kN/mm, and also more flexible than the Ansys L Fixed. This relation was expected, since the Ansys L Fixed model considers both slip modulus of the connection,  $8 \frac{kN}{mm}$  near the fixed support and  $23.2 \frac{kN}{mm}$  on the rest of the beam, hence its equivalent beam effective stiffness is in between the two analytical models.

The good agreement of the Analytical 8 kN with the Ansys NL model shown in Figure 3.8, thus with the test result, is believed to be a coincidence, since neither the fixed support behavior, the non linear behavior of the concrete nor the correct distribution of the connection slip modulus along the beam were considered in this analytical model. However, further experimental data is required before concluding remarks.

To consider the correct distribution of the connection slip modulus along the beam in the Girhammar method, it is proposed to replace the slip modulus of the connection with an effective slip modulus. The recommendation is equivalent to the one made by EC5 (European Committee for Standardization, 1995) for the case when the spacing of the fasteners varies along the longitudinal axis of the beam, and it can be seen in the following equation:

$$k_{eff} = 0.75k_{tension} + 0.25k_{compression} \quad (3.1)$$

where  $k_{tension}$ ,  $k_{compression}$  and  $k_{eff}$  are the slip modulus obtained through the test where the concrete is in tension, the slip modulus obtained through the test where the concrete is in compression (traditional push-out test) and the effective slip modulus respectively. Figure 3.9 shows a comparison between the mentioned procedure (Proposed Analytical in the legend) and the Ansys L model. A good agreement between the results was found using the proposed effective slip modulus, since at a load of 120 kN a difference of 6 % of the deflection prediction was found between the proposed method and the Ansys L model.

Figure 3.10 shows the slip between the concrete and timber at 80 kN load for the test results, the Ansys L Fixed, Ansys NL and the Analytical model prediction. For the Analytical model, the results shown from 0 m to 2.9 m relate to the results of the Analytical 8kN/mm model, while the results of the Analytical 23 kN/mm model were plotted from 2.9 to 4.0 m. The mentioned distances correspond to the inflection point of the moment diagram on a propped cantilever beam, since at 2.9 m from the simple support the moment changes sign.

A good agreement between the numerical results and the test results can be observed in Figure 3.10, even though they tend to underestimate the slip between 0 and 2.0 m, and overestimate it between 2.0 and 4.0 m. The Ansys NL predicts accurately the slip at the simple support, underestimate it by 37.5% at 1.0 m and overestimate it by 25% at 3.0 m. Additionally, the difference between a perfectly fixed support and the actual support

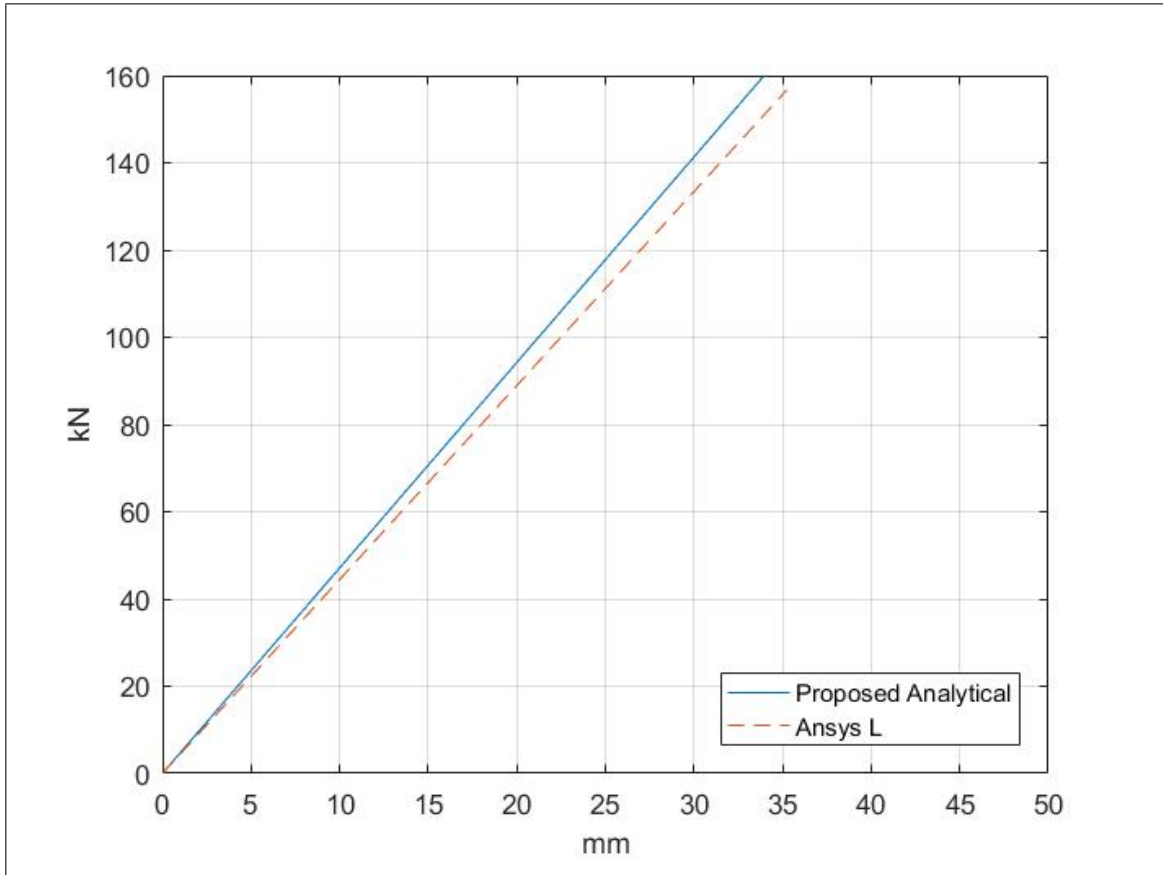


Figure 3.9. Comparison of maximum deflection calculated with the Proposed analytical model and Ansys L model.

conditions of the test can be observed at 4.0 m, where the Ansys L Fixed model predict 0.0 mm of slip, but the test results and the Ansys NL model predict slips of -0.25 mm and -0.48 mm respectively.

Since the approximation given by Girhammar (2009) to obtain the interlayer force is proportional to the shear force  $V$ , the interlayer slip behaves equally. Thus, it can be observed from Figure 3.10 a piecewise linear prediction of the interlayer slip by the analytical model, similar to the test results or the numerical prediction between 0 and 2.9 m. In the first 2 m the analytical model underestimates the interlayer slip by up 41% maximum. At 3 m the analytical model overestimates the slip by 145%. Between 2.9 and 4.0 m the analytical model largely overestimates the slip, which was expected since even

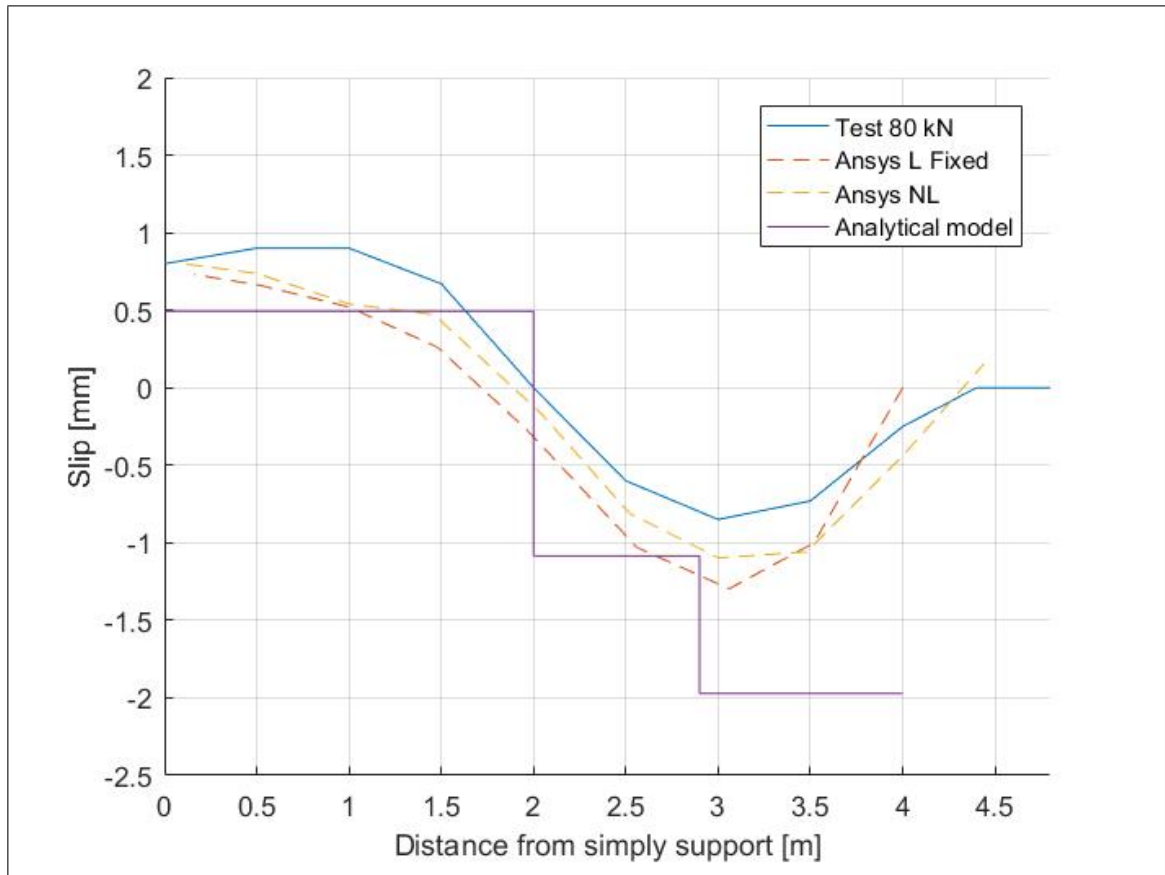


Figure 3.10. Slip along the beam at 80 kN Load. Test results adapted from Sebastian et al. (2016).

though the shear force is maximum over the fixed support, the interlayer slip is negligible, and then Equation 2.14 fails estimating the value of slip near fixed supports. However, considering the maximum interlayer slip obtained with the analytical model is always conservative.

#### 4. PROPOSAL OF DESIGN PROCEDURE

The objective of this section is to present a design procedure for a TCC system under different boundary conditions in accordance with the methods presented earlier. The procedure is based on the current standard (European Committee for Standardization, 1995), but modified with the provisions given in this thesis, and it will be explained through a design example in Section 4.1. The procedure is divided in two main sections: ultimate limit states (ULS) and serviceability limit states (SLS), according with the requirements of EC5 (European Committee for Standardization, 1995). The proposed design procedure is summarized in Figure 4.2 and 4.3, and a comparison between the proposed design procedure and the provisions given by the current standard EC5 is shown in Table 4.1. For more details about the design according to the provisions of EC5 (European Committee for Standardization, 1995), a design example was developed by Dias et al. (2018).

Table 4.1. Comparison between the proposed design procedure and the EC5 design procedure.

Variable	Proposed design procedure	EC5 design procedure (European Committee for Standardization, 1995)
Design method	Girhammar method	$\gamma$ - method
Boundary conditions different to simply supported	Yes	No
Statically indeterminate systems	Yes	No
Load distribution	It can consider any load distribution	Only uniformly distributed loads
Environmental conditions	It considers varying environmental conditions through the Toratti model and CEB 90 model	It considers only one environmental condition through the assignment of a Service Class (only 3 classes)
Concrete creep factor	Calculated through the CEB 90 model	From tables depending of the Service Class
Timber creep factor	Calculated using the Toratti model	From tables depending of the Service Class and type of timber
Connection creep factor	Considering $2\phi_w$	Considering $2\phi_w$
Concrete shrinkage contribution	Yes, through the formulas shown in Appendix A	No
Evolution of the deflection over time	Yes	No, just the instant and final deflection

The difference of the proposed design procedure with the traditional design according to the requirements of EC5, is that EC5 suggest the use of the  $\gamma$ -method (Section 2.1) regardless the boundary conditions of the beam, simply adjusting the length of the beam to 0.8 times the span for continuous beams, and to twice the span for cantilever beams (European Committee for Standardization, 1995). On the other hand, in the proposed design procedure it is suggested to use the Girhammar method (Section 2.2) for boundary conditions different to simply supported. The equations of the method were explained in Section 2.2 and can be observed in equations 4.1, 4.2, 4.3, 4.4, 4.5, 4.6, 4.7, 4.8, 4.9, 4.9 and 4.10. The properties of the cross section are shown in Figure 4.1.

$$EI_{eff} = \left[ 1 + \frac{\frac{EI_{\infty} - 1}{EI_0}}{1 + \left(\frac{\mu}{\pi}\right)^2 (\alpha L)^2} \right]^{-1} EI_{\infty} \quad (4.1)$$

$$\alpha = \sqrt{\frac{K d^2}{EI_0 \left(1 - \frac{EI_0}{EI_{\infty}}\right)}} \quad (4.2)$$

$$EI_0 = E_1 I_1 + E_2 I_2 \quad (4.3)$$

$$EA_0 = E_1 A_1 + E_2 A_2 \quad (4.4)$$

$$EA_p = E_1 A_1 \cdot E_2 A_2 \quad (4.5)$$

$$EI_{\infty} = EI_0 + \frac{EA_p d^2}{EA_0} \quad (4.6)$$

$$F_{s,eff} = \left(1 - \frac{EI_0}{EI_{eff}}\right) \frac{Vs}{d} \quad (4.7)$$

$$\sigma_{i,eff,max} = \sigma_i \mp \sigma_{i,b} = \left[ \left( 1 - \frac{EI_0}{EI_{eff}} \right) \frac{1}{A_i d} \mp \frac{E_i h_i}{2EI_{eff}} \right] M \quad (4.8)$$

$$\tau_{i,eff,max} = \frac{E_i h_{na,i,eff}^2}{2EI_{eff}} V \quad (4.9)$$

$$h_{na,i,eff} = \min \left\{ \begin{array}{l} h_i \\ \frac{h_i}{2} + \left( 1 - \frac{EI_0}{EI_{eff}} \right) \frac{EI_{eff}}{E_i A_i d} \end{array} \right. \quad (4.10)$$

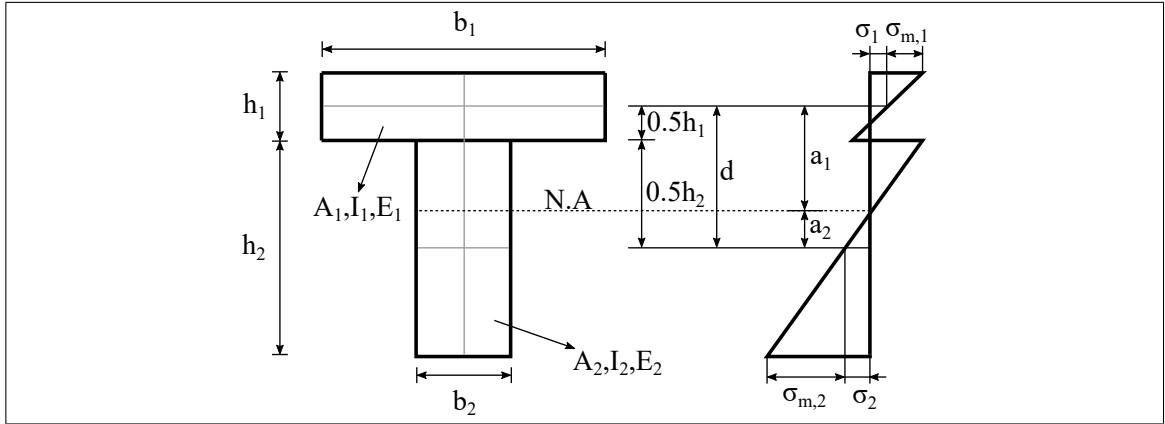


Figure 4.1. Cross section (left) and stress distribution (right) of a TCC.

For the long-term behavior, the main difference between the proposed procedure and the EC5 design procedure is that in the first one the effects of the concrete shrinkage are considered through the formulas presented in Appendix A, while in the second one it is not considered. Additionally, the proposed design procedure takes into account the inelastic strains due to hygrometric variations, whereas the EC5 does not. The procedure where explained in Section 2.3, while the equations are the following:

$$E_{c,eff}^i = \frac{E_c(t_i)}{1 + \Phi_c(t, t_i)} \quad (4.11)$$

$$E_{w,eff}^i = \frac{E_w(t_i)}{1 + \Phi_w(t, t_i)} \quad (4.12)$$

$$k_{f,eff}^i = \frac{k_f(t_i)}{1 + 2\Phi_w(t, t_i)} \quad (4.13)$$

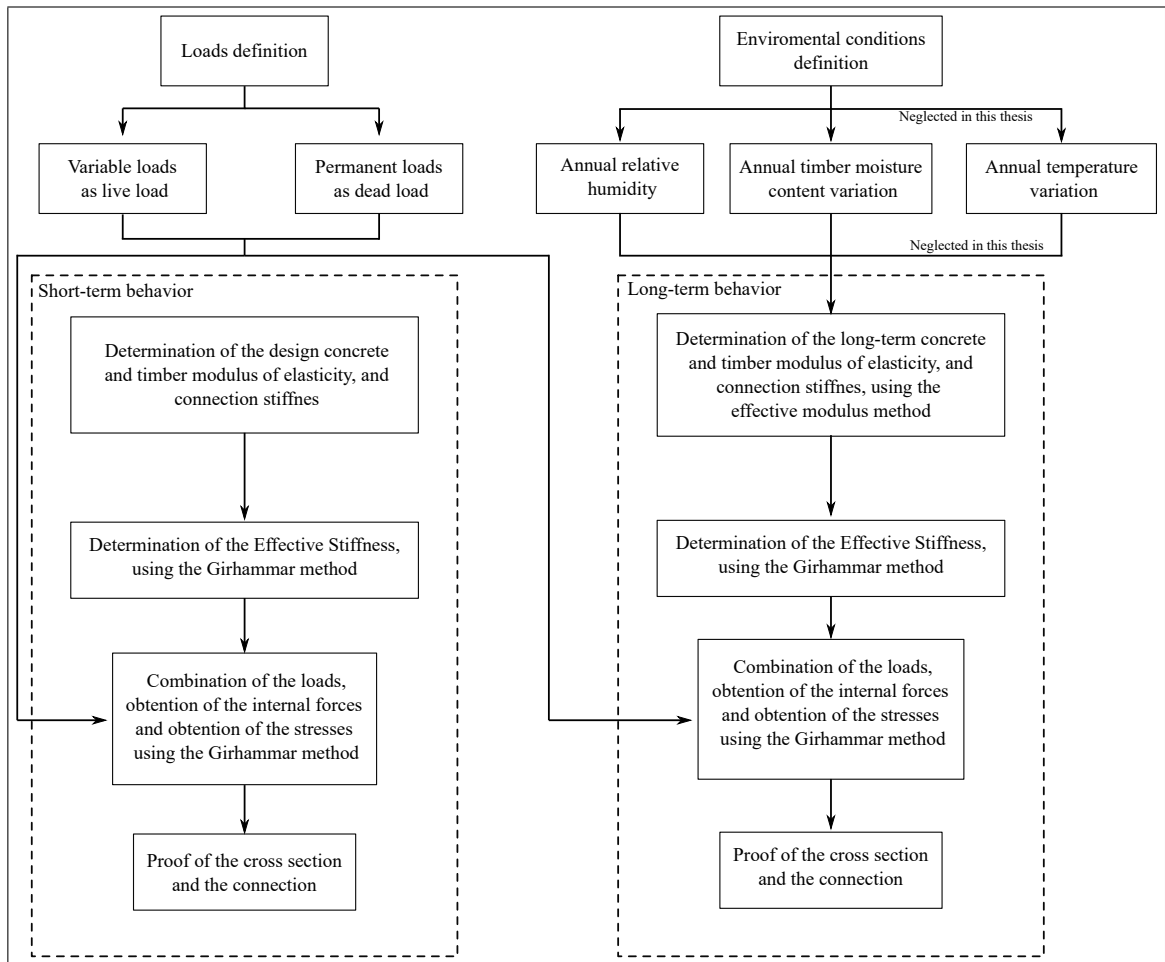


Figure 4.2. Summary of the proposed design procedure for the Ultimate Limit States

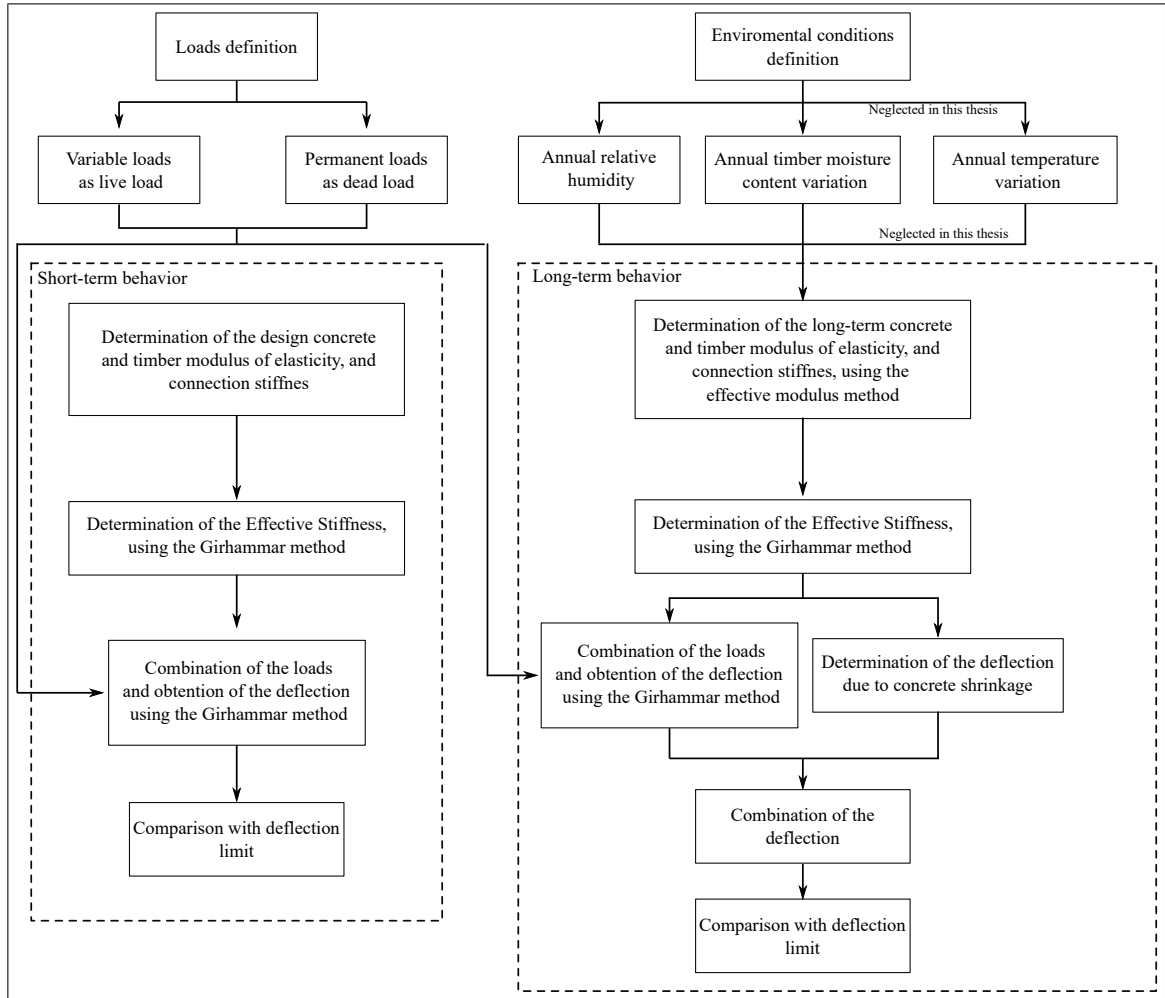


Figure 4.3. Summary of the proposed design procedure for the Serviceability Limit States.

#### 4.1. Design example

A design example is shown in this section, according to the provisions given in this thesis, and using the current standard, EN1995-1-1 (1995). The geometry of the slab is shown in Figure 4.4, and the material properties are in accordance with the ones presented in Section 3.1.

Regarding the considerations made for this procedure, the remarks of ACI318-14 (American Concrete Institute, 2014) was used for the deflection limits, since they are

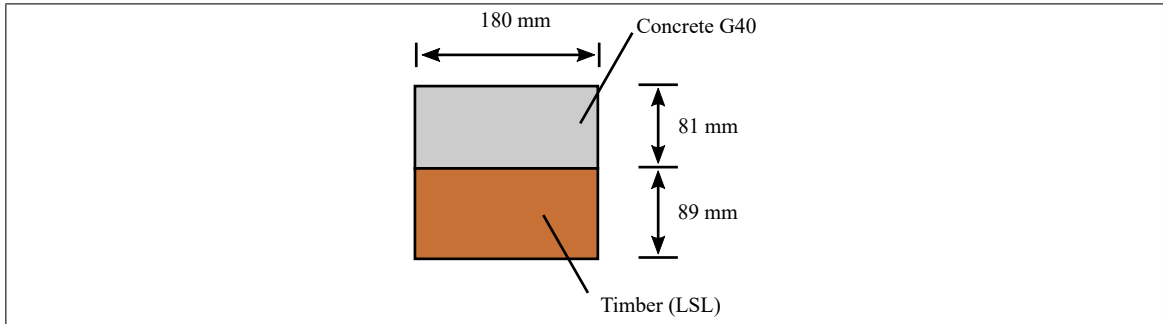


Figure 4.4. Slab design.

more restrictive than EC5 (European Committee for Standardization, 1995). The modification factors to obtain the timber and concrete design forces were obtained from EC5 (European Committee for Standardization, 1995) and EC2 (European Committee for Standardization, 1992), while a very conservative assumption was made to obtain the design force for the connectors.

#### 4.1.1. Basic information

##### 4.1.1.1. Cross section dimensions and properties

Concrete depth:	$h_1 = 81 \text{ mm}$	Figure 4.4
Concrete width:	$b_1 = 180 \text{ mm}$	Figure 4.4
Concrete Area:	$A_1 = b_1 h_1 = 14.58 \times 10^3 \text{ mm}^2$	
Concrete second moment of area:	$I_1 = b_1 \frac{h_1^3}{12} = 79.71 \times 10^5 \text{ mm}^4$	
Timber depth:	$h_2 = 89 \text{ mm}$	Figure 4.4
Timber width:	$b_2 = 180 \text{ mm}$	Figure 4.4
Timber Area:	$A_2 = b_2 h_2 = 16.02 \times 10^3 \text{ mm}^2$	
Timber second moment of area:	$I_2 = b_2 \frac{h_2^3}{12} = 10.57 \times 10^6 \text{ mm}^4$	
Distance between both neutral axis:	$d = \frac{h_1}{2} + \frac{h_2}{2} = 85 \text{ mm}$	Figure 4.1

#### 4.1.1.2. Connection properties

Type of fasteners:	Rothoblaas VB 7.5 x 100	
Diameter:	$d_1 = 7.5 \text{ mm}$	(Rothoblaas, n.d.)
Fastener length:	$l_1 = 145 \text{ mm}$	(Rothoblaas, n.d.)
Penetration length:	$l_{ef} = 100 \text{ mm}$	(Rothoblaas, n.d.)
Fastener inclination:	$\alpha = 45^\circ$	
Slip modulus for a pair of VB:	$K_{ser} = 240l_{ef} = 24000 \frac{N}{mm}$	(Rothoblaas, n.d.)
Tensile capacity for a pair of VB:	$f_{tens,k} = 16 \text{ kN}$	(Rothoblaas, n.d.)
Spacing between the fasteners:	$s = 240 \text{ mm}$	
Fasteners per row:	2	

#### 4.1.1.3. Concrete properties

Concrete type :	Normal weight concrete	
Compressive strength at 28 days:	$f'_c = 41 \text{ MPa}$	
Tensile strength:	$f_t = 0.62\sqrt{f'_c} = 3.97 \text{ MPa}$	(American Concrete Institute, 2014)
Modulus of elasticity:	$E_c = 4700\sqrt{f'_c} = 30095 \text{ MPa}$	(American Concrete Institute, 2014)
Characteristic density:	$\rho_1 = 2400 \frac{kg}{m^3}$	(American Concrete Institute, 2014)
Partial factor:	$\gamma_c = 1.5$	(European Committee for Standardization, 1992)

#### 4.1.1.4. Timber properties

Timber type:	Laminated Strand Lumber	(Louisiana Pacific Corporation, 2019)
Bending strength:	$f_{b,0} = 17.24 \text{ MPa}$	(Louisiana Pacific Corporation, 2019)
Tensile strength:	$f_{t,0} = 0.6f_{b,0} = 10.344 \text{ MPa}$	(European Committee for Standardization, 2009)
Modulus of elasticity:	$E_t = 12065 \text{ MPa}$	(Louisiana Pacific Corporation, 2019)
Shear strength:	$f_v = 2.83 \text{ MPa}$	(Louisiana Pacific Corporation, 2019)
Compression strength parallel to grain:	$f_{ct} = 16.82 \text{ MPa}$	(Louisiana Pacific Corporation, 2019)
Characteristic density:	$\rho_2 = 770 \frac{kg}{m^3}$	(Louisiana Pacific Corporation, 2019)

Service class:	1 (residential building)	(European Committee for Standardization, 1995)
Partial factor:	$\gamma_m = 1.2$	(European Committee for Standardization, 1995)
Partial factor:	$k_{mod} = 0.8$ (medium term action)	(European Committee for Standardization, 1995)

#### 4.1.1.5. Loads and Load Combinations

Self weight:	$SW = 2.56 \text{ kPa}$	
Dead Load:	$D = 0.981 \text{ kPa}$	
Live Load:	$L = 1.962 \text{ kPa}$	
SLS short-term load combination:	$SW + D + L$	(European Committee for Standardization, 1990)
SLS long-term load combination:	$SW + D + 0.3L$	(European Committee for Standardization, 1990)
ULS short-term load combination:	$1.35(SW + D) + 1.5L$	(European Committee for Standardization, 1990)
ULS long-term load combination:	$1.35(SW + D) + 1.5L$	(European Committee for Standardization, 1990)

#### 4.1.1.6. Internal forces analysis

Figure 4.5 shows the shear and moment diagram of a propped cantilever beam. These diagrams were used above to obtain the design shear and moment values.

Boundary conditions:	Fixed end & simply supported end.
Permanent Load:	$q_D = (D + SW)b_1 = 0.64 \frac{N}{mm}$
Variable Load:	$q_L = Lb_1 = 0.35 \frac{N}{mm}$
Load for the ULS:	$q = 1.35q_D + 1.5q_L = 1.39 \frac{N}{mm}$
ULS positive bending moment:	$M_{max} = \frac{9}{128}qL^2 = 3.52 \text{ kNm}$
ULS negative bending moment:	$M_B = -\frac{1}{8}qL^2 = 6.26 \text{ kNm}$
ULS maximum design shear force:	$V_B = \frac{5}{8}qL = 5.21 \text{ kN}$
ULS minimum design shear force:	$V_B = \frac{3}{8}qL = 3.13 \text{ kN}$

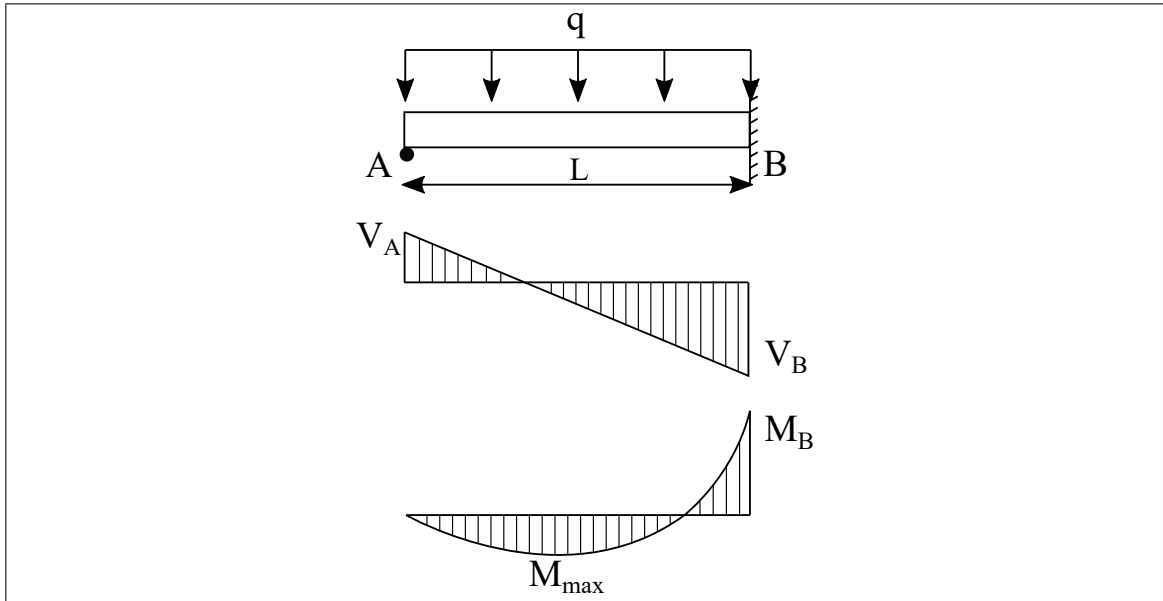


Figure 4.5. Moment and shear diagram of a propped cantilever beam.

#### 4.1.2. Verification of the ultimate limit state at the short-term

##### 4.1.2.1. Material properties

Concrete modulus of elasticity:  $E_1 = E_c = 30095 \text{ MPa}$

Timber modulus of elasticity:  $E_2 = E_t = 12065 \text{ MPa}$

Connection slip modulus:  $k_u = \frac{2}{3}k_{ser} = 16000 \frac{\text{N}}{\text{mm}}$

(European Committee for Standardization, 1995)

##### 4.1.2.2. Effective bending stiffness

Bending stiffness of the non composite section:  $EI_0 = 3.68 \times 10^{11} \text{ Nmm}^2$

Equation 4.3

Bending stiffness of the fully composite section:  $EI_\infty = 13.37 \times 10^{11} \text{ Nmm}^2$

Equation 4.6

$\alpha$  value:  $\alpha = 0.0013 \frac{1}{\text{mm}}$

Equation 4.2

Effective bending stiffness:  $EI_{eff} = 8.23 \times 10^{11} \text{ Nmm}^2$

Equation 4.1

#### 4.1.2.3. Concrete normal stresses at the mid-span

Normal stress:	$\sigma_1 = \left(1 - \frac{EI_0}{EI_{eff}}\right) \frac{1}{A_1 d} M_{max} = 1.58 \text{ MPa}$	Equation 4.8
Bending stress:	$\sigma_{1,b} = \left(\frac{E_1 h_1}{2EI_{eff}}\right) M_{max} = 5.23 \text{ MPa}$	Equation 4.8
Stress at the top:	$\sigma_{1,top} = -\sigma_1 - \sigma_{1,b} = -6.81 \text{ MPa}$	
Stress at the bottom:	$\sigma_{1,bot} = -\sigma_1 + \sigma_{1,b} = 3.65 \text{ MPa}$	
Design compressive strength:	$f_{c,d} = \frac{f'_c}{\gamma_c} = 27.33 \text{ MPa}$	(European Committee for Standardization, 1992)
Design tensile strength:	$f_{t,d} = \frac{f_t}{\gamma_c} = 2.65 \text{ MPa}$	(European Committee for Standardization, 1992)
Compressive safety factor:	$\frac{\sigma_{1,bot}}{f_{c,d}} = \frac{6.81}{27.33} = 0.25 \leq 1$	Satisfied
Tensile safety factor:	$\frac{\sigma_{1,top}}{f_{t,d}} = \frac{3.65}{2.65} = 1.38 > 1$	Require steel reinforcement

#### 4.1.2.4. Concrete normal stresses at the fixed support

Normal stress:	$\sigma_1 = \left(1 - \frac{EI_0}{EI_{eff}}\right) \frac{1}{A_1 d} M_B = -2.8 \text{ MPa}$	Equation 4.8
Bending stress:	$\sigma_{1,b} = \left(\frac{E_1 h_1}{2EI_{eff}}\right) M_B = -9.3 \text{ MPa}$	Equation 4.8
Stress at the top:	$\sigma_{1,top} = -\sigma_1 - \sigma_{1,b} = 12.1 \text{ MPa}$	
Stress at the bottom:	$\sigma_{1,bot} = -\sigma_1 + \sigma_{1,b} = -6.5 \text{ MPa}$	
Design compressive strength:	$f_{c,d} = \frac{f'_c}{\gamma_c} = 27.33 \text{ MPa}$	(European Committee for Standardization, 1995)
Design tensile strength:	$f_{t,d} = \frac{f_t}{\gamma_c} = 2.65 \text{ MPa}$	(European Committee for Standardization, 1995)
Compressive safety factor:	$\frac{\sigma_{1,bot}}{f_{c,d}} = \frac{6.5}{27.33} = 0.24 \leq 1$	Satisfied
Tensile safety factor:	$\frac{\sigma_{1,top}}{f_{t,d}} = \frac{12.1}{2.65} = 4.6 > 1$	Require steel reinforcement

#### 4.1.2.5. Timber normal stresses at the mid-span

Normal stress:	$\sigma_2 = \left(1 - \frac{EI_0}{EI_{eff}}\right) \frac{1}{A_2 d} M_{max} = 1.43 \text{ MPa}$	Equation 4.8
Bending stress:	$\sigma_{2,b} = \left(\frac{E_2 h_2}{2EI_{eff}}\right) M_{max} = 2.3 \text{ MPa}$	Equation 4.8
Stress at the top:	$\sigma_{2,top} = \sigma_2 - \sigma_{2,b} = -0.87 \text{ MPa}$	
Stress at the bottom:	$\sigma_{2,bot} = \sigma_2 + \sigma_{2,b} = 3.73 \text{ MPa}$	
Design tensile strength:	$f_{t,td} = k_{mod} \frac{f_{t,0}}{\gamma_m} = 11.49 \text{ MPa}$	(European Committee for Standardization, 1995)
Design bending strength:	$f_{b,td} = k_{mod} \frac{f_{b,0}}{\gamma_m} = 6.9 \text{ MPa}$	(European Committee for Standardization, 1995)

Compressive safety factor:	$\frac{\sigma_{2,top}}{f_{t,cd}} = \frac{0.87}{11.21} = 0.08 \leq 1$	Satisfied
Flexural tensile safety factor:	$\frac{\sigma_2}{f_{t,td}} + \frac{\sigma_{2,b}}{f_{b,td}} = \frac{1.43}{11.49} + \frac{2.3}{6.9} = 0.46 \leq 1$	Satisfied

#### 4.1.2.6. Timber normal stresses at the fixed support

Normal stress:	$\sigma_2 = \left(1 - \frac{EI_0}{EI_{eff}}\right) \frac{1}{A_2 d} M_B = -2.55 \text{ MPa}$	Equation 4.8
Bending stress:	$\sigma_{2,b} = \left(\frac{E_2 h_2}{2EI_{eff}}\right) M_B = -4.1 \text{ MPa}$	Equation 4.8
Stress at the top:	$\sigma_{2,top} = \sigma_2 - \sigma_{2,b} = 1.55 \text{ MPa}$	
Stress at the bottom:	$\sigma_{2,bot} = \sigma_2 + \sigma_{2,b} = -6.65 \text{ MPa}$	
Design compressive strength:	$f_{t,cd} = k_{mod} \frac{f_{ct}}{\gamma_m} = 11.21 \text{ MPa}$	(European Committee for Standardization, 1995)
Design bending strength:	$f_{b,td} = k_{mod} \frac{f_{b,0}}{\gamma_m} = 6.9 \text{ MPa}$	(European Committee for Standardization, 1995)
Compressive safety factor:	$\frac{\sigma_{2,bot}}{f_{t,cd}} = \frac{4.74}{11.21} = 0.42 \leq 1$	Satisfied
Flexural compressive safety factor:	$\frac{\sigma_2}{f_{c,td}} + \frac{\sigma_{2,b}}{f_{b,td}} = \frac{2.55}{11.21} + \frac{4.1}{6.9} = 0.82 \leq 1$	Satisfied

#### 4.1.2.7. Timber shear stress

Distance to neutral axis:	$h_{na,2,eff} = 72.2 \text{ mm}$	Equation 4.10
Shear stress:	$\tau_{i,eff,max} = \frac{E_2 h_{na,i,eff}^2}{2EI_{eff}} V_B = 0.2 \text{ MPa}$	Equation 4.9
Design shear strength:	$f_{v,td} = k_{mod} \frac{f_v}{\gamma_m} = 1.89 \text{ MPa}$	(European Committee for Standardization, 1995)
Shear strength safety factor:	$\frac{\tau_{i,eff,max}}{f_{v,td}} = 0.1 \leq 1$	Satisfied

#### 4.1.2.8. Connection shear strength

Since it has been found that the use of Equation 2.14 lead to overestimate the loads in the connectors at the fixed-end (see Table 3.4), it is proposed to verify the shear force at the simply supported end, to obtain a more realistic value of the load.

Shear load at the simply support:	$V_A = 3.13 \text{ kN}$	
Load on the fasteners:	$F_{s,eff} = \left(1 - \frac{EI_0}{EI_{eff}}\right) \frac{V_A s}{d} = 4.9 \text{ kN}$	Equation 4.7
Design load capacity:	$f_{tens,des} = \frac{1}{3} f_{tens,k} = 5.33 \text{ kN}$	(Clouston & Schreyer, 2008)

Shear safety factor:  $\frac{F_{s,eff}}{f_{tens,des}} = \frac{4.9}{5.33} = 0.92 \leq 1$  Satisfied

### 4.1.3. Verification of the ultimate limit state at the long-term

#### 4.1.3.1. Material properties

Concrete creep coefficient:	$\phi_c(50years) = 2.18$	(Comité Euro-International du Béton, 1993)
Timber creep coefficient:	$\phi_w(50years) = 0.94$	(Toratti, 1993)
Connection creep coefficient:	$\phi_f(50years) = 1.88$	(Toratti, 1993)
Concrete modulus of elasticity:	$E_1 = \frac{E_c}{1+\phi_c(50)} = 9447.1 MPa$	Equation 4.11
Timber modulus of elasticity:	$E_2 = \frac{E_t}{1+\phi_w(50)} = 6198.6 MPa$	Equation 4.12
Connection slip modulus:	$k = \frac{k_{ser}}{1+2\phi_f(50)} = 8296.4 \frac{N}{mm}$	Equation 4.13

#### 4.1.3.2. Effective bending stiffness

Bending stiffness of the non composite section:	$EI_0 = 1.41 \times 10^{11} Nmm^2$	Equation 4.3
Bending stiffness of the fully composite section:	$EI_\infty = 5.58 \times 10^{11} Nmm^2$	Equation 4.6
$\alpha$ value:	$\alpha = 0.0015 \frac{1}{mm}$	Equation 4.2
Effective bending stiffness:	$EI_{eff} = 3.56 \times 10^{11} Nmm^2$	Equation 4.1

#### 4.1.3.3. Concrete normal stresses at the mid-span

Normal stress:	$\sigma_1 = \left(1 - \frac{EI_0}{EI_{eff}}\right) \frac{1}{A_1 d} M_{max} = 1.72 MPa$	Equation 4.8
Bending stress:	$\sigma_{1,b} = \left(\frac{E_1 h_1}{2EI_{eff}}\right) M_{max} = 3.79 MPa$	Equation 4.8
Stress at the top:	$\sigma_{1,top} = -\sigma_1 - \sigma_{1,b} = -5.51 MPa$	
Stress at the bottom:	$\sigma_{1,bot} = -\sigma_1 + \sigma_{1,b} = 2.07 MPa$	
Design compressive strength:	$f_{c,d} = \frac{f'_c}{\gamma_c} = 27.33 MPa$	(European Committee for Standardization, 1992)
Design tensile strength:	$f_{t,d} = \frac{f_t}{\gamma_c} = 2.65 MPa$	(European Committee for Standardization, 1992)

Compressive safety factor:  $\frac{\sigma_{1,bot}}{f_{c,d}} = \frac{5.51}{27.33} = 0.2 \leq 1$  Satisfied

Tensile safety factor:  $\frac{\sigma_{1,top}}{f_{t,d}} = \frac{2.07}{2.65} = 0.78 \leq 1$  Satisfied

#### 4.1.3.4. Concrete normal stresses at the fixed support

Normal stress:  $\sigma_1 = \left(1 - \frac{EI_0}{EI_{eff}}\right) \frac{1}{A_1 d} M_B = -3.06 \text{ MPa}$  Equation 4.8

Bending stress:  $\sigma_{1,b} = \left(\frac{E_1 h_1}{2EI_{eff}}\right) M_B = -6.74 \text{ MPa}$  Equation 4.8

Stress at the top:  $\sigma_{1,top} = -\sigma_1 - \sigma_{1,b} = 9.8 \text{ MPa}$

Stress at the bottom:  $\sigma_{1,bot} = -\sigma_1 + \sigma_{1,b} = -3.68 \text{ MPa}$

Design compressive strength:  $f_{c,d} = \frac{f'_c}{\gamma_c} = 27.33 \text{ MPa}$  (European Committee for Standardization, 1995)

Design tensile strength:  $f_{t,d} = \frac{f_t}{\gamma_c} = 2.65 \text{ MPa}$  (European Committee for Standardization, 1995)

Compressive safety factor:  $\frac{\sigma_{1,bot}}{f_{c,d}} = \frac{3.68}{27.33} = 0.13 \leq 1$  Satisfied

Tensile safety factor:  $\frac{\sigma_{1,top}}{f_{t,d}} = \frac{9.8}{2.65} = 3.70 > 1$  Require steel reinforcement

#### 4.1.3.5. Timber normal stresses at the mid-span

Normal stress:  $\sigma_2 = \left(1 - \frac{EI_0}{EI_{eff}}\right) \frac{1}{A_2 d} M_{max} = 1.57 \text{ MPa}$  Equation 4.8

Bending stress:  $\sigma_{2,b} = \left(\frac{E_2 h_2}{2EI_{eff}}\right) M_{max} = 2.73 \text{ MPa}$  Equation 4.8

Stress at the top:  $\sigma_{2,top} = \sigma_2 - \sigma_{2,b} = -1.16 \text{ MPa}$

Stress at the bottom:  $\sigma_{2,bot} = \sigma_2 + \sigma_{2,b} = 4.3 \text{ MPa}$

Design tensile strength:  $f_{t,td} = k_{mod} \frac{f_{t,0}}{\gamma_m} = 11.49 \text{ MPa}$  (European Committee for Standardization, 1995)

Design bending strength:  $f_{b,td} = k_{mod} \frac{f_{b,0}}{\gamma_m} = 6.9 \text{ MPa}$  (European Committee for Standardization, 1995)

Compressive safety factor:  $\frac{\sigma_{2,top}}{f_{t,cd}} = \frac{1.16}{11.21} = 0.1 \leq 1$  Satisfied

Flexural tensile safety factor:  $\frac{\sigma_2}{f_{t,td}} + \frac{\sigma_{2,b}}{f_{b,td}} = \frac{1.57}{11.49} + \frac{2.73}{6.9} = 0.53 \leq 1$  Satisfied

#### 4.1.3.6. Timber normal stresses at the fixed support

Normal stress:  $\sigma_2 = \left(1 - \frac{EI_0}{EI_{eff}}\right) \frac{1}{A_2 d} M_B = -2.79 \text{ MPa}$  Equation 4.8

Bending stress:  $\sigma_{2,b} = \left(\frac{E_2 h_2}{2EI_{eff}}\right) M_B = -4.86 \text{ MPa}$  Equation 4.8

Stress at the top:  $\sigma_{2,top} = \sigma_2 - \sigma_{2,b} = 2.07 \text{ MPa}$

Stress at the bottom:  $\sigma_{2,bot} = \sigma_2 + \sigma_{2,b} = -7.65 \text{ MPa}$

Design compressive strength:	$f_{t,cd} = k_{mod} \frac{f_{ct}}{\gamma_m} = 11.21 \text{ MPa}$	(European Committee for Standardization, 1995)
Design bending strength:	$f_{b,td} = k_{mod} \frac{f_{b,0}}{\gamma_m} = 6.9 \text{ MPa}$	(European Committee for Standardization, 1995)
Compressive safety factor:	$\frac{\sigma_{2,bot}}{f_{t,cd}} = \frac{7.65}{11.21} = 0.68 \leq 1$	Satisfied
Flexural compressive safety factor:	$\frac{\sigma_2}{f_{c,td}} + \frac{\sigma_{2,b}}{f_{b,td}} = \frac{2.79}{11.21} + \frac{4.86}{6.9} = 0.95 \leq 1$	Satisfied

#### 4.1.3.7. Timber shear stress

Distance to neutral axis:	$h_{na,2,eff} = 70.00 \text{ mm}$	Equation 4.10
Shear stress:	$\tau_{i,eff,max} = \frac{E_2 h_{na,i,eff}^2}{2EI_{eff}} V_B = 0.13 \text{ MPa}$	Equation 4.9
Design shear strength:	$f_{v,td} = k_{mod} \frac{f_v}{\gamma_m} = 1.89 \text{ MPa}$	(European Committee for Standardization, 1995)
Shear strength safety factor:	$\frac{\tau_{i,eff,max}}{f_{v,td}} = 0.07 \leq 1$	Satisfied

#### 4.1.3.8. Connection shear strength

Since it has been found that the use of Equation 2.14 lead to overestimate the loads in the connectors (see Table 3.4) at the fixed end, it is proposed to verify the shear force at the simply supported end, to obtain a more realistic value of the load.

Shear load at the simply support:	$V_A = 3.13 \text{ kN}$	
Load on the fasteners:	$F_{s,eff} = \left(1 - \frac{EI_0}{EI_{eff}}\right) \frac{V_A s}{d} = 5.33 \text{ kN}$	Equation 4.7
Design load capacity:	$f_{tens,des} = \frac{1}{3} f_{tens,k} = 5.33 \text{ kN}$	(Clouston & Schreyer, 2008)
Shear safety factor:	$\frac{F_{s,eff}}{f_{tens,des}} = \frac{5.33}{5.33} = 1 \leq 1$	Satisfied

### 4.1.4. Verification of the serviceability limit state at the short-term

#### 4.1.4.1. Material properties

Concrete modulus of elasticity:  $E_1 = E_c = 30095 \text{ MPa}$

Timber modulus of elasticity:  $E_2 = E_t = 12065 \text{ MPa}$

Connection slip modulus:  $k = k_{ser} = 24000 \frac{N}{mm}$

#### 4.1.4.2. Effective bending stiffness

Bending stiffness of the non composite section:  $EI_0 = 3.68 \times 10^{11} \text{ Nmm}^2$  Equation 4.3

Bending stiffness of the fully composite section:  $EI_\infty = 13.37 \times 10^{11} \text{ Nmm}^2$  Equation 4.6

$\alpha$  value:  $\alpha = 0.0016 \frac{1}{mm}$  Equation 4.2

Effective bending stiffness:  $EI_{eff} = 9.2 \times 10^{11} \text{ Nmm}^2$  Equation 4.1

#### 4.1.4.3. Deflection

Deflection of the slab:  $w_{inst} = \frac{(q_D + q_L)L^4}{185EI_{eff}} = 7.56 \text{ mm}$  Figure 2.2

Deflection limit:  $w_{max} = \frac{L}{480} = 12.5 \text{ mm}$  (American Concrete Institute, 2014)

Deflection safety factor:  $\frac{w_{inst}}{w_{max}} = 0.6 \leq 1$  Satisfied

#### 4.1.5. Verification of the serviceability limit state at the long-term

##### 4.1.5.1. Material properties

Concrete creep coefficient:  $\phi_c(50years) = 2.18$  (Comité Euro-International du Béton, 1993)

Timber creep coefficient:  $\phi_w(50years) = 0.94$  (Toratti, 1993)

Connection creep coefficient:  $\phi_f(50years) = 1.88$  (Toratti, 1993)

Concrete modulus of elasticity:  $E_1 = \frac{E_c}{1 + \phi_c(50)} = 9447.1 \text{ MPa}$  Equation 4.11

Timber modulus of elasticity:  $E_2 = \frac{E_t}{1 + \phi_w(50)} = 6198.6 \text{ MPa}$  Equation 4.12

Connection slip modulus:  $k = \frac{k_{ser}}{1 + 2\phi_f(50)} = 8296.4 \text{ MPa}$  Equation 4.13

#### 4.1.5.2. Effective bending stiffness

Bending stiffness of the non composite section:  $EI_0 = 1.41 \times 10^{11} \text{ Nmm}^2$  Equation 4.3

Bending stiffness of the fully composite section:  $EI_\infty = 5.58 \times 10^{11} \text{ Nmm}^2$  Equation 4.6

$\alpha$  value:  $\alpha = 0.0015 \frac{1}{\text{mm}}$  Equation 4.2

Effective bending stiffness:  $EI_{eff} = 3.56 \times 10^{11} \text{ Nmm}^2$  Equation 4.1

#### 4.1.5.3. Deflection

Deflection of the slab:  $w_{LT} = \frac{(q_D + 0.3q_L)L^4}{185EI_{eff}} = 14.69 \text{ mm}$

Deflection due to concrete shrinkage:  $w_{sh} = 3.92 \text{ mm}$

Total deflection:  $w_{total} = w_{LT} + w_{sh} = 18.61 \text{ mm}$

Deflection limit:  $w_{max} = \frac{L}{480} = 12.5 \text{ mm}$

Deflection safety factor:  $FF_w = \frac{w_{total}}{w_{max}} = 1.49 > 1$

Figure 2.2

Appendix A

(American Concrete Institute, 2014)

Not satisfied

Since the deflection safety factor is not satisfied, it is suggested to apply a precambering of 10 mm to fulfill the requirements of ACI318-14 (American Concrete Institute, 2014).

## 5. CONCLUSIONS

An analytical and numerical analysis about TCC slabs subjected to boundary conditions different than simply supported was proposed in this thesis. The prediction of deflection, stresses and internal forces by the proposed analytical models were compared with different numerical models. Lastly, an analytical design procedure was proposed considering the results shown in this thesis, and a design example of a slab for a residential building in Chile was developed. The main conclusions of this thesis are presented in the next paragraphs.

Considering that the FE models are able to reproduce the observed behavior of a TCC, and that the analytical models (such as Girhammar) results are in good agreement with the FEM ones, it can be concluded that the hypothesis is true. The objective of developing an analytical method for analysis and design of TCC floor slabs under boundary conditions different than simply supported was achieved. The models were described in Section 2, validated numerically and experimentally in Section 3, and the proposed design procedure was explained and detailed through a design example in Section 4.

The Girhammar method provided a good approximation of the deflection compared with nonlinear and linear short-term numerical models, regardless the boundary conditions of the slab. Additionally, for a propped cantilever slab subjected to service loads, the stresses obtained with the Girhammar method were in good agreement with the ones obtained with numerical models. The mid-term (5 years) and long-term (50 years) deflections obtained with the proposed analytical method were in good agreement with the numerical results, regardless the boundary conditions.

The proposed analytical model was validated with experimental results available in the literature. It was found through numerical models that the experimental setup reported in Sebastian et al. (2016) did not provide a perfectly fixed support. Thus, the deflection predicted by the Girhammar method considering a fixed end did not provide a good estimation of the maximum deflection. Since the prediction of the Girhammar method highly

depends on the boundary conditions, it is important for designing to consider the proper support conditions, to obtain a realistic prediction of the behavior of the slab.

Without considering the fixed end, where the slip tends to zero, the shear force  $F_s$  obtained with the Girhammar method for a distributed load was in good agreement with numerical results. However, the analytical model did not provide a good estimation of the interlayer slip reported by Sebastian et al. (2016), while the numerical models results were closer. More experimental data is needed to study this behavior, which should be reinforced with a study of the local effects near the shear connectors (neglected in this research).

Changing the boundary conditions of a slab from simply supported to propped cantilever can reduce the long-term deflection by 50%. Thus, the deflection of the slab can be reduced without pre-cambering or increasing the thickness, but changing the support conditions. As it was proved in this thesis, it is possible to design a TCC slab considering the requirements of a Chilean real state, proving its feasibility and making it competitive with a traditional concrete slab.

Since the experimental data of TCC slabs subjected to boundary conditions different to simply supported is scarce, more experimental campaigns are needed in order to validate the proposed design method. In order to start implementing this composite floor system in reinforced concrete buildings, further research is needed, including the following:

- (i) Short-term and long-term (at least 3 years) experimental campaigns regarding the behavior of TCC slabs with boundary conditions different to simply supported.
- (ii) Theoretical and experimental campaigns regarding the dynamic behavior (seismic) of TCC slabs regardless the boundary conditions.
- (iii) Theoretical and experimental campaigns regarding the connection of the TCC slabs to reinforced concrete shear walls.

## REFERENCES

- American Concrete Institute. (2014). *Building Code Requirements for Structural Concrete (ACI 318-14) and Commentary (ACI 318R-14)*. Farmington Hills.
- Balogh, J., Fragiaco, M., Gutkowski, R., Atadero, R., & Ivanyi, P. (2013). Low-to-high cycle fatigue behavior of wood-concrete composite beams with notched interlayer connections. *Pollack Periodica*, 8(1), 3–14. doi: 10.1556/Pollack.8.2013.1.1
- Bathon, L. A., & Bletz, O. (2006). Long term performance of continuous wood-concrete-composite systems. In *9th world conference on timber engineering 2006, wcte 2006* (pp. 502–507).
- Boccardo, L., Zweidler, S., Steiger, R., & Frangi, A. (2017). Bending tests on timber-concrete composite members made of beech laminated veneer lumber with notched connection. *Engineering Structures*, 132, 14–28. Retrieved from <http://dx.doi.org/10.1016/j.engstruct.2016.11.029> doi: 10.1016/j.engstruct.2016.11.029
- Brunner, M., Romer, M., & Schnüriger, M. (2007). Timber-concrete-composite with an adhesive connector (wet on wet process). *Materials and Structures/Materiaux et Constructions*, 40(1), 119–126. doi: 10.1617/s11527-006-9154-4
- Ceccotti, A. (2002). Composite concrete-timber structures. *Progress in Structural Engineering and Materials*, 4(3), 264–275. doi: 10.1002/pse.126
- Ceccotti, A., Fragiaco, M., & Giordano, S. (2007). Long-term and collapse tests on a timber-concrete composite beam with glued-in connection. *Materials and Structures/Materiaux et Constructions*, 40(1), 15–25. doi: 10.1617/s11527-006-9094-z
- Clouston, P., & Schreyer, A. (2008). Design and Use of Wood Concrete Composites. , *13*(November), 167–174. doi: 10.1061/(ASCE)1084-0680(2008)13

Comité Euro-International du Béton. (1993). *CEB-FIP MODEL CODE 1990*. Thomas Telford Publishing. Retrieved from <http://www.icevirtuallibrary.com/doi/book/10.1680/ceb-fipmc1990.35430> doi: 10.1680/ceb-fipmc1990.35430

Dias, A., Schänzlin, J., & Dietsch, P. (2018). *Design of timber-concrete composite structures: A state-of-the-art report by COST Action FP1402 / WG 4* (Tech. Rep.).

Dias, A. M., Van de Kuilen, J. W., Lopes, S., & Cruz, H. (2007). A non-linear 3D FEM model to simulate timber-concrete joints. *Advances in Engineering Software*, 38(8-9), 522–530. doi: 10.1016/j.advengsoft.2006.08.024

European Committee for Standardization. (1990). *Eurocode- Basis of structural design* (No. 2010).

European Committee for Standardization. (1992). *Eurocode2: Design of concrete structures - Part 1-1: General rules and rules for buildings* (No. 2004).

European Committee for Standardization. (1995). *Eurocode 5: Design of timber structures - Part 1-1: General - Common rules and rules for buildings* (No. 2005).

European Committee for Standardization. (2009). *UNI EN 338: Structural timber Strength classes - British Standards Institute*. doi: 10.1016/j.jglr.2014.11.012

European Committee for Standardization. (2011). *Eurocode 5: Design of timber structures - Part 1-2: General - Structural fire design* (No. 2005).

Fragiacomo, M. (2006). Long-term behavior of timber-concrete composite beams. II: Numerical analysis and simplified evaluation. *Journal of Structural Engineering*, 132(1), 23–33. doi: 10.1061/(ASCE)0733-9445(2006)132:1(23)

Fragiacomo, M. (2012). Experimental behaviour of a full-scale timber-concrete composite floor with mechanical connectors. *Materials and Structures/Materiaux et Constructions*,

45(11), 1717–1735. doi: 10.1617/s11527-012-9869-3

Fragiacomo, M., & Ceccotti, A. (2006a). Long-term behavior of timber-concrete composite beams. I: Finite element modeling and validation. *Journal of Structural Engineering*, 132(1), 13–22. doi: 10.1061/(ASCE)0733-9445(2006)132:1(13)

Fragiacomo, M., & Ceccotti, A. (2006b). Simplified approach for the long-term behaviour of timber-concrete composite beams according to the Eurocode 5 provisions. In *International council for research and innovation in building and construction*. Retrieved from <https://ir.canterbury.ac.nz/handle/10092/18>

Fragiacomo, M., Gutkowski, R. M., Balogh, J., & Fast, R. S. (2007). Long-term behavior of wood-concrete composite floor/deck systems with shear key connection detail. *Journal of Structural Engineering*, 133(9), 1307–1315. doi: 10.1061/(ASCE)0733-9445(2007)133:9(1307)

Girhammar, U. A. (2009). A simplified analysis method for composite beams with interlayer slip. *International Journal of Mechanical Sciences*, 51(7), 515–530. Retrieved from <http://dx.doi.org/10.1016/j.ijmecsci.2009.05.003>  
doi: 10.1016/j.ijmecsci.2009.05.003

Girhammar, U. A., & Pan, D. H. (2007). Exact static analysis of partially composite beams and beam-columns. *International Journal of Mechanical Sciences*, 49(2), 239–255. doi: 10.1016/j.ijmecsci.2006.07.005

Gutkowski, R., Brown, K., Shigidi, A., & Natterer, J. (2008). Laboratory tests of composite wood-concrete beams. *Construction and Building Materials*, 22(6), 1059–1066. doi: 10.1016/j.conbuildmat.2007.03.013

Gutkowski, R. M., Balogh, J., & To, L. G. (2010). Finite-element modeling of short-term field response of composite wood-concrete floors/decks. *Journal of Structural Engineering*, 136(6), 707–714. doi: 10.1061/(ASCE)ST.1943-541X.0000117

Instituto Nacional de Normalización. (2009). *NCh 1537. Of2009 - Diseño estructural - Cargas permanentes y cargas de uso.*

Jiang, Y., & Crocetti, R. (2019). CLT-concrete composite floors with notched shear connectors. *Construction and Building Materials*, 195. doi: 10.1016/j.conbuildmat.2018.11.066

Khorsandnia, N., Valipour, H., & Crews, K. (2014). Structural response of timber-concrete composite beams predicted by finite element models and manual calculations. *Advances in Structural Engineering*, 17(11), 1601–1621. doi: 10.1260/1369-4332.17.11.1601

Khorsandnia, N., Valipour, H., Schänzlin, J., & Crews, K. (2016). Experimental Investigations of Deconstructable Timber-Concrete Composite Beams. *Journal of Structural Engineering*, 142(12), 1–13. doi: 10.1061/(ASCE)ST.1943-541X.0001607

Khorsandnia, N., Valipour, H. R., Shrestha, R., Gerber, C., & Crews, K. (2013). Review on long-term behaviour of timber-concrete composite floors. In *From materials to structures: Advancement through innovation - proceedings of the 22nd australasian conference on the mechanics of structures and materials, acmsm 2012* (pp. 1053–1058). doi: 10.1201/b15320-188

Lopes, S., Jorge, L., & Cruz, H. (2012). Evaluation of non-linear behavior of timber-concrete composite structures using FE model. *Materials and Structures/Materiaux et Constructions*, 45(5), 653–662. doi: 10.1617/s11527-011-9787-9

Louisiana Pacific Corporation. (2019). *LP SolidStart LSL Beam & Header Technical Guide* (Tech. Rep.). Louisiana Pacific Corporation. Retrieved from <https://lpcorp.com/resources/product-literature?product=SolidStartLSL>

Lukaszewska, E. (2009). *Development of Prefabricated Timber-Concrete Floors* (Doctoral dissertation, Lulea University of Technology). Retrieved from <https://www.google.com/url?sa=>

t{&}rct=j{&}q={&}esrc=s{&}source=web{&}cd={&}ved=  
2ahUKEwiy9ILqvdrrAhX6D7kGHTikCx8QFjACegQIARAB{&}url=  
https{&}3A{&}2F{&}2Fwww.diva-portal.org{&}2Fsmash{&}2Fget{&}2Fdiva2{&}  
.pdf{&}usg=AOvVaw3REcqyumN43nBM442HkaZY

Lukaszewska, E., Fragiaco, M., & Johnsson, H. (2010). Laboratory tests and numerical analyses of prefabricated timber-concrete composite floors. *Journal of Structural Engineering*, 136(1), 46–55. doi: 10.1061/(ASCE)ST.1943-541X.0000080

Marchi, L. (2018). *Innovative connection systems for timber structures* (Doctoral dissertation, Università degli Studi di Padova). Retrieved from <http://paduaresearch.cab.unipd.it/11111/>

Mudie, J., Sebastian, W. M., Norman, J., & Bond, I. P. (2019). Experimental study of moment sharing in multi-joist timber-concrete composite floors from zero load up to failure. *Construction and Building Materials*, 225, 956–971. Retrieved from <https://doi.org/10.1016/j.conbuildmat.2019.07.137> doi: 10.1016/j.conbuildmat.2019.07.137

Müller, K., & Frangi, A. (2018). 4-Point Bending Tests of Timber-Concrete Composite Slabs With Micro-Notches. In *Wcte 2018 - world conference on timber engineering* (pp. 1–7).

Rodrigues, J. N., Dias, A. M., & Providência, P. (2013). Timber-concrete composite bridges: State-of-the-art review. *BioResources*, 8(4), 6630–6649. doi: 10.15376/biores.8.4.6630-6649

Rothoblaas. (n.d.). *VB. Conector for wood-concrete floors* (Tech. Rep.). SFS in-tec. Retrieved from <https://www.rothoblaas.es/productos/fijacion/tornillos/tornillos-estructuras/vb>

Sebastian, W., Mudie, J., Cox, G., Piazza, M., Tomasi, R., & Giongo, I. (2016, jan).

Insight into mechanics of externally indeterminate hardwoodconcrete composite beams. *Construction and Building Materials*, 102, 1029–1048. Retrieved from <https://linkinghub.elsevier.com/retrieve/pii/S0950061815304372> doi: 10.1016/j.conbuildmat.2015.10.015

Tannert, T., Ebadi, M. M., & Gerber, A. (2019). Serviceability Performance of Timber Concrete Composite Floors. In *Modular and offsite construction (moc) summit proceedings* (pp. 206–212). doi: 10.29173/mocs95

Tannert, T., Endacott, B., Brunner, M., & Vallée, T. (2017). Long-term performance of adhesively bonded timber-concrete composites. *International Journal of Adhesion and Adhesives*, 72(October 2016), 51–61. Retrieved from <http://dx.doi.org/10.1016/j.ijadhadh.2016.10.005> doi: 10.1016/j.ijadhadh.2016.10.005

Toratti, T. (1993). Long Term Deflection of Timber Beams. *Journal of Structural Mechanics*, 26(3), 19–28.

Yeoh, D., Fragiacomio, M., Buchanan, A., & Gerber, C. (2009). Preliminary research towards a semi-prefabricated LVL-concrete composite floor system for the Australasian market. *Australian Journal of Structural Engineering*, 9(3), 225–240. doi: 10.1080/13287982.2009.11465025

Yeoh, D., Fragiacomio, M., De Franceschi, M., & Heng Boon, K. (2011). State of the art on timber-concrete composite structures: Literature review. *Journal of Structural Engineering*, 137(10), 1085–1095. doi: 10.1061/(ASCE)ST.1943-541X.0000353

Yeoh, D., Fragiacomio, M., & Deam, B. (2011, sep). Experimental behaviour of LVLconcrete composite floor beams at strength limit state. *Engineering Structures*, 33(9), 2697–2707. Retrieved from <https://linkinghub.elsevier.com/retrieve/pii/S0141029611002215> doi: 10.1016/j.engstruct.2011.05.021

Zona, A., Barbato, M., & Fragiacomio, M. (2012). Finite-Element model updating and

probabilistic analysis of Timber-concrete composite Beams. *Journal of Structural Engineering*, 138(7), 899–910. doi: 10.1061/(ASCE)ST.1943-541X.0000509

## **APPENDIX**

## A. ELASTIC ANALYSIS OF INELASTIC STRAINS FOR DIFFERENT BOUNDARY CONDITIONS

In this appendix it is shown the analytical procedure to quantify deflection due to an imposed deformation in a sub component of a TCC. Specifically, the procedure is oriented to obtain the closed-form solution of a fixed end- simply supported beam. However, the solution can be obtained for every kind of support state, applying the correspondent boundary conditions.

The area and bending stiffness of the beam sub components "i" are assumed uniform along the element, i.e.,  $E(x)_i I(x)_i = E_i I_i$  and  $A(x)_i = A_i$ . Consider and imposed uniform deformation  $\varepsilon_{imp,i}$  on each sub component of the beam, and assume that vertical separation between the concrete and timber is restricted.

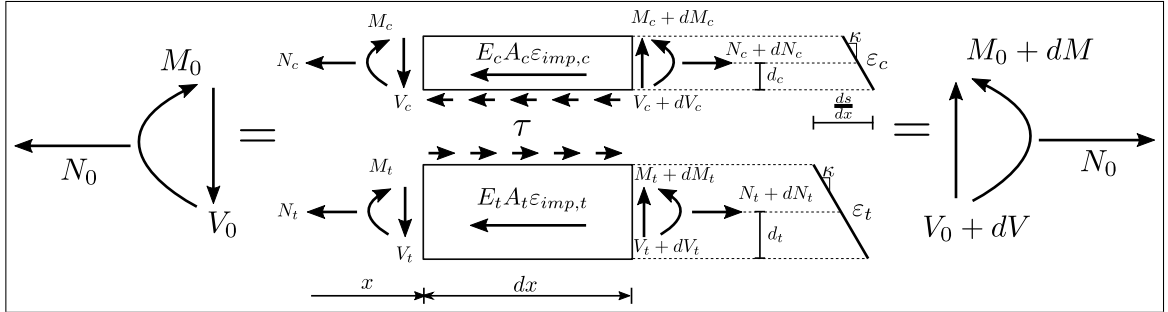


Figure A.1. Differential element of a TCC subjected to axial deformations of each component.

Consider the differential element shown in Figure A.1. From the right part of the Figure, the slip strain can be defined as:

$$\frac{ds}{dx} = \varepsilon_c - \varepsilon_t + \kappa d \quad (\text{A.1})$$

where  $d = d_c + d_t$  and the curvature of the beam is assumed to be:

$$\kappa = \frac{M_c}{E_c I_c} = \frac{M_t}{E_t I_t} \quad (\text{A.2})$$

Linear behavior is assumed for all materials. Therefore:

$$\varepsilon_c = \frac{N_c}{E_c A_c} \quad (\text{A.3})$$

$$\varepsilon_t = \frac{N_t}{E_t A_t} \quad (\text{A.4})$$

From the global equilibrium of the structure, three equations can be obtained:

$$M_0 + M_c + M_t - N_c d - E_c A_c \varepsilon_{imp,c} d = 0 \quad (\text{A.5})$$

$$N_0 + N_c + N_t + E_c A_c \varepsilon_{imp,c} + E_t A_t \varepsilon_{imp,t} = 0 \quad (\text{A.6})$$

$$V_c + V_t + V_0 = 0 \quad (\text{A.7})$$

If linear behavior is assumed in the connection, the force per unit length at the interface can be defined as:

$$\tau = K s \quad (\text{A.8})$$

Then, from the differential equilibrium of the structure, the following relations can be obtained:

$$\frac{dM_c}{dx} = -V_c + \tau d_c \quad (\text{A.9})$$

$$\frac{dM_t}{dx} = -V_t + \tau d_t \quad (\text{A.10})$$

$$\frac{dN_c}{dx} = \tau \quad (\text{A.11})$$

$$\frac{dN_t}{dx} = -\tau \quad (\text{A.12})$$

Adding the equation A.9 and A.10:

$$\frac{dM_c}{dx} + \frac{dM_t}{dx} = V_0 + \tau d \quad (\text{A.13})$$

From A.2 and A.7, the previous equation can be expressed as

$$\frac{d\kappa}{dx} = \frac{V_0}{EI_0} + \frac{\tau d}{EI_0} \quad (\text{A.14})$$

where  $EI_0 = EI_c + EI_t$ . The equation A.1 can be differentiated once again in order to use the equation A.8, A.11, A.12 and A.14:

$$\frac{d^2 s}{dx^2} = \alpha^2 s + \beta \quad (\text{A.15})$$

where  $\alpha = K(\frac{1}{EI_c} + \frac{1}{EI_t} + \frac{1}{EI_0})$ , and  $\beta = \frac{V_0}{EI_0}d$ , which can be considered as constant. The solution of the equation A.15 set out the relative slip between the concrete and timber, and can be expressed as:

$$s(x) = C_1 [\cosh(\alpha x) + \sinh(\alpha x)] + C_2 [\cosh(\alpha x) - \sinh(\alpha x)] - \frac{\beta}{\alpha^2} \quad (\text{A.16})$$

where  $C_1$  and  $C_2$  are constants which depend of the boundary conditions. Given the boundary conditions of a propped cantilever beam,

$$s(x = 0) = 0 \quad (\text{A.17})$$

$$\frac{ds}{dx}(x = L) = \Delta\varepsilon \quad (\text{A.18})$$

with  $\Delta\varepsilon = \varepsilon_{imp,t} - \varepsilon_{imp,c}$ . Solving  $C_1$  and  $C_2$ , the slip between the concrete and timber can be expressed as:

$$s(x) = \beta \left[ \cosh(\alpha(L - x)) - \frac{1}{\alpha^2} \right] + \Delta\varepsilon \frac{\sinh(\alpha x)}{\alpha \cosh(\alpha L)} \quad (\text{A.19})$$

The equation A.19 and A.8 can be replaced in A.14, obtaining:

$$\frac{d\kappa}{dx} = \frac{\beta}{d} + \frac{Ks(x)d}{EI_0} \quad (\text{A.20})$$

The differential equation A.20 can be solved by applying boundary conditions. Since this model is aimed to a propped cantilever beam, it can be said that  $\kappa(x = L) = 0$ . Said that,

$$\begin{aligned} \kappa(x) = & - \left(1 - \frac{EI_0}{EI_{inf}}\right) \frac{1}{\alpha d} \left[ \Delta\varepsilon \alpha - \beta \alpha (L - x) + \beta \frac{\sinh(\alpha(L - x))}{\cosh(\alpha L)} - \Delta\varepsilon \frac{\alpha \cosh(\alpha x)}{\cosh(\alpha L)} \right] \\ & - \beta \frac{(L - x)}{d} \end{aligned} \quad (\text{A.21})$$

where  $EI_{inf} = EI_0 + EA^*d^2$ ,  $EA^* = \frac{EA_p}{EA_0}$ ,  $EA_p = EA_c \cdot EA_t$  and  $EA_0 = EA_c + EA_t$ . Additionally, the deflection of the beam can be derived by integrating twice the equation A.21, since  $w(x) = \int \theta(x)dx = \int \int \kappa(x)dx^2$ :

$$w(x) = C_4 + C_3x + \frac{x^2}{2d} \left( -\Delta\varepsilon \left( 1 - \frac{EI_0}{EI_\infty} \right) - \beta \frac{EI_0}{EI_\infty} \left( L - \frac{x}{3} \right) \right) - \left( 1 - \frac{EI_0}{EI_{inf}} \right) \frac{\beta \sinh(L-x) - \alpha \Delta\varepsilon \cosh(\lambda x)}{\alpha^3 d \cosh(\alpha L)} \quad (\text{A.22})$$

To obtain the values of the constants  $C_1$ ,  $C_2$  and  $\beta$ , the following set of boundary conditions has to be used in equation A.22:

$$w(x=0) = 0 \quad (\text{A.23})$$

$$w(x=L) = L \quad (\text{A.24})$$

$$\theta(x=0) = 0 \quad (\text{A.25})$$

Replacing the previous conditions in equation A.22:

$$C_3 = \frac{3\Delta\varepsilon (EI_\infty - EI_0)^2 [\cosh(\alpha L) (\alpha^2 L^2 - 2) + 2]}{2EI_\infty \alpha d [3(EI_\infty - EI_0) (\alpha L \cosh(\alpha L) - \sinh(\alpha L)) + EI_0 L^3 \alpha^3 \cosh(\alpha L)]} \quad (\text{A.26})$$

$$C_4 = \frac{-\Delta\varepsilon (EI_\infty - EI_0) [(\sinh(\alpha L) (\alpha^2 L^2 - 2) + 6\alpha L) (EI_\infty - EI_0) + 2EI_0 L^3 \alpha^3]}{2EI_\infty \alpha^2 d [3(EI_\infty - EI_0) (\alpha L \cosh(\alpha L) - \sinh(\alpha L)) + EI_0 L^3 \alpha^3 \cosh(\alpha L)]} \quad (\text{A.27})$$

$$\beta = \frac{-3\alpha \Delta\varepsilon (EI_\infty - EI_0) [\cosh(\alpha L) (\alpha^2 L^2 - 2) + 2]}{2 [3(EI_\infty - EI_0) (\alpha L \cosh(\alpha L) - \sinh(\alpha L)) + EI_0 L^3 \alpha^3 \cosh(\alpha L)]} \quad (\text{A.28})$$

## B. COMPARISON OF CREEP MODELS FOR CONCRETE AND TIMBER

This appendix contains a comparison between the Toratti creep model (Toratti, 1993) and CEB 90 creep model (Comité Euro-International du Béton, 1993) with the adjusted model used in Ansys. The value of the constants used for each analysis are in a table above each figure. The analysis was done for five and fifty years since concrete casting.

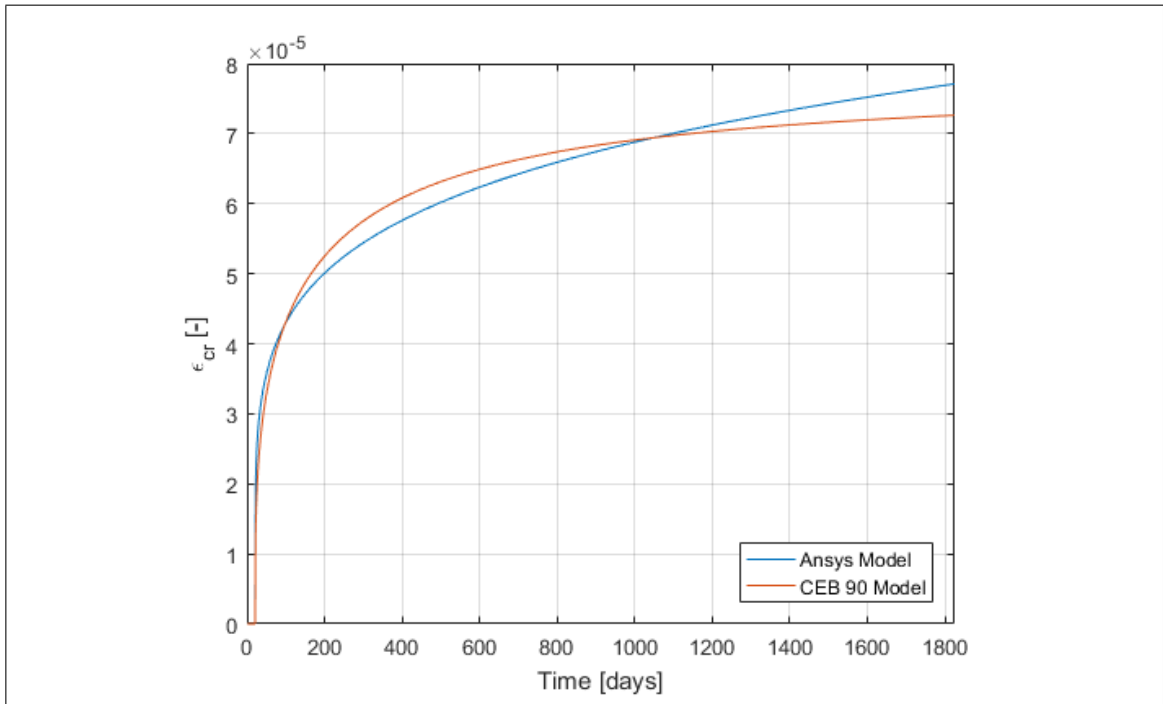


Figure B.1. Concrete creep model comparison for five years.

Table B.1. Constant values for concrete creep model for five years.

Constant	Value
$C_1$	$4.25 \times 10^{-7}$
$C_2$	1
$C_3$	-0.813
$C_4$	0

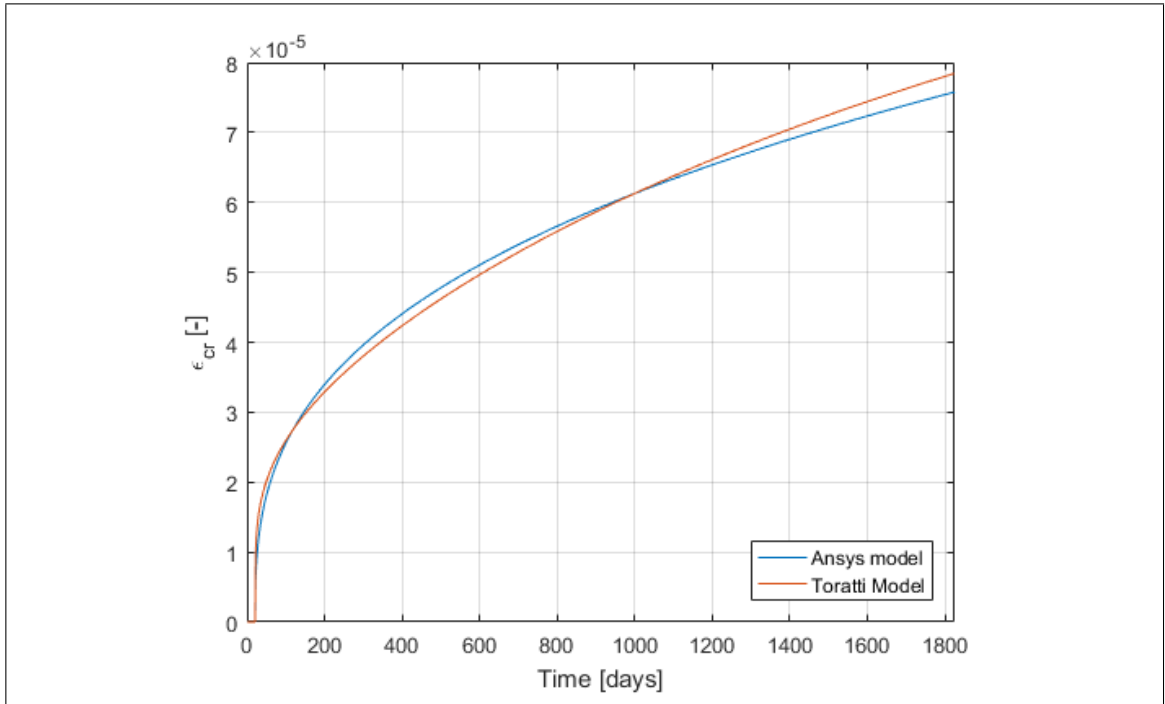


Figure B.2. Timber creep and mechanosorptive model comparison for five years.

Table B.2. Constant values for concrete creep model for five years.

Constant	Value
$C_1$	$3.74 \times 10^{-8}$
$C_2$	1
$C_3$	-0.652
$C_4$	0

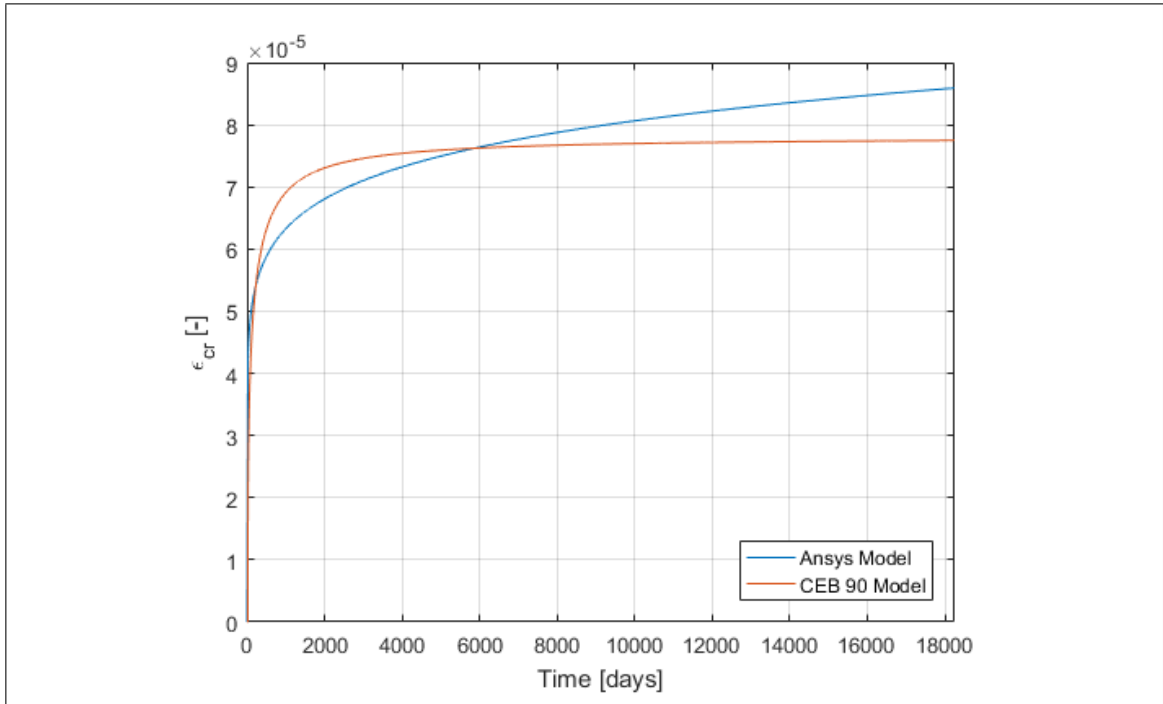


Figure B.3. Concrete creep model comparison for fifty years.

Table B.3. Constant values for concrete creep model for fifty years.

Constant	Value
$C_1$	$9.72 \times 10^{-7}$
$C_2$	1
$C_3$	-0.895
$C_4$	0

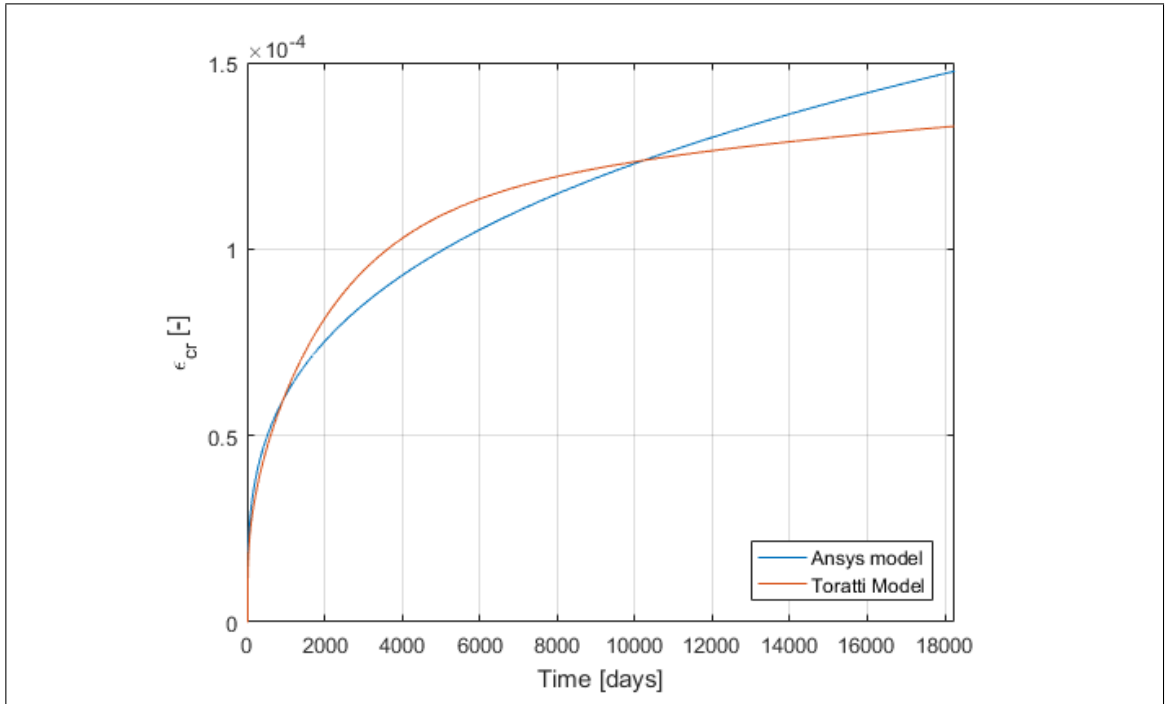


Figure B.4. Timber creep and mechanosorptive model comparison for fifty years.

Table B.4. Constant values for concrete creep model for fifty years.

Constant	Value
$C_1$	$7.02 \times 10^{-8}$
$C_2$	1
$C_3$	-0.695
$C_4$	0